The Lunar Mare Ring-Moat Dome Structure (RMDS) Age Conundrum: Contemporaneous with Imbrian-Aged Host Lava Flows or Emplaced in the Copernican?

Feng Zhang[1,2], James W. Head[3], Christian Wöhler[4], Alexander T. Basilevsky[5], Lionel Wilson[6], Minggang Xie[7], Roberto Bugiolacchi[2], Thorsten Wilhelm[4], Stephanie Althoff[4], and Yong L. Zou[1]

[1]State Key Laboratory of Space Weather, National Space Science Center, Chinese Academy of Sciences, Beijing, China; [2]State Key Laboratory of Lunar and Planetary Sciences, Macau University of Science and Technology, Macau, China; [3]Department of Earth, Environmental and Planetary Sciences, Brown University, Providence, RI, USA; [4]Image Analysis Group, TU Dortmund University, Dortmund, Germany; [5]Vernadsky Institute of Geochemistry and Analytical Chemistry, Russian Academy of Sciences, Moscow, Russia; [6]Lancaster Environment Centre, Lancaster University, Lancaster, UK; [7]College of Science, Guilin University of Technology, Guilin, China

Corresponding Author: F. Zhang (zhangfeng@nssc.ac.cn)

Key Points:

(1) Clusters of unusual features, Ring Moat Dome Structures (RMDSs), occur extensively in the lunar maria

(2) Multiple lines of evidence suggest two alternative origins, contemporaneous with Imbrian flows, or later, in the Copernican

(3) We list outstanding questions and suggest future research and exploration scenarios to resolve the age conundrum

Abstract

Ring-Moat Dome Structures (RMDSs) are small circular mounds of diameter typically about 200 m and ~3-4 m in height, surrounded by narrow, shallow moats. They occur in clusters, are widespread in ancient Imbrian-aged mare basalt host units and show mineralogies comparable to those of their host units. Based on these close associations and similarities, a model has been proposed for the formation of RMDS as the result of late-stage flow inflation, with second boiling releasing quantities of

magmatic volatiles that migrate to the top of the flow as magmatic foams and extrude through cracks in the cooled upper part of the flow to produce the small RMDS domes and surrounding moats. In contrast to this model advocating a contemporaneous emplacement of RMDSs and their host lava flows, a range of observations suggests that the RMDS formed significantly after the emplacement and cooling of their host lava flows, perhaps as recently as in the Copernican Period (~1.1 Ga to the present). These observations include: 1) stratigraphic embayment of domes into post-lava flow emplacement impact craters; 2) young crater degradation age estimates for the underlying embayed craters; 3) regolith development models that predict thicknesses in excess of the observed topography of domes and moats; 4) landform diffusional degradation models that predict very young ages for mounds and moats; 5) suggestions of fewer superposed craters on the mounds than on the adjacent host lava flows, and 6) observations of superposed craters that suggest that the mound substrate does not have the properties predicted by the magmatic foam model. Together, these observations are consistent with the RMDS formation occurring during the period after the extrusion and solidification of the host lava flows, up to and including the geologically recent Late Copernican, i.e., the last few hundreds of millions of years of lunar history. We present and discuss each of these contradictory data and interpretations and summarize the requirements for magma ascent and eruption models that might account for young RMDS ages. We conclude with a discussion of the tests and future research and exploration that might help resolve the

RMDS age and mode of emplacement conundrum.

Plain Language Summary

The research reported in this paper provides multiple lines of evidence for the discovery of very young mare volcanism on the Moon, thus extending the lunar volcanic history into the Copernican period (~1.1 Ga to present). Current lunar thermal evolution models have placed an upper limit for the cessation of large-scale mare volcanism at ~2.0 Ga ago. In this study, we used both morphometric analysis and topographic diffusion models to date some small craters (100-300 m in scale) which are partially overlapped by ring-moat dome structures (RMDSs, basaltic lava flow surface features characterized by a domical profile encircled by a ring moat). Our results lead to a conclusion that lunar mare volcanism accounting for the emplacement of these RMDS-bearing basalts may have occurred several hundreds of millions of years ago (i.e., 130-1500 Ma), thus challenging the present consensus on the thermal history of the Moon. To address this issue, we also list a series of outstanding questions and robotic/human exploration strategies that could provide conclusive evidence for or against our hypotheses, thus increasing our understanding of the duration and flux of lunar volcanism and the thermal evolution of the Moon.

1. Introduction

A major outstanding question in the evolution of the Moon is the onset, duration and flux of lunar mare volcanism, and its contribution to the building of the lunar secondary crust. The study of lunar meteorites shows that volcanism started early in the history of the Moon (> 4 Ga) (Borg et al., 2015; Taylor et al., 1983; Terada et al., 2007); however, much less consensus has been reached on the time of cessation of extrusive activities. This is not a secondary issue: a reliable timeline would constrain our current models of the thermal and compositional evolution of the Moon (e.g., Head, 1976; Hess & Parmentier, 1995; Solomon, 1978, 1986; Wieczorek et al., 2006). Returned lunar samples indicate that the bulk of mare volcanism was confined to the interval of 3.8 to 3.1 Ga years ago, with major volcanic eruptions peaking in the Imbrian period (3.8-3.2 Ga ago; Head & Wilson, 2017; Hiesinger et al., 2011). The youngest ages of lunar mare volcanism have been reported in the range of ~2.9/2.5 Ga from the study of lunar meteorites (Borg et al., 2004; Fernandes et al., 2007), and, by inference, as young as 1.2 Ga from crater chronology approaches based on the comparison with lunar chronology functions (Hiesinger et al., 2011; Schultz & Spudis, 1983). Even younger ages of ~10 Ma relating to the Ina structure (Schultz et al., 2006) and <100 Ma for Ina-like irregular mare patches (IMPs) (Braden et al., 2014) have been put forward based on this indirect approach. However, Ina and its surrounding mare are compositionally identical (Bennett et al., 2015), making the likelihood of being geologically contemporaneous most likely (Garry et al., 2012; Qiao et al., 2017; Wilson & Head, 2017b). Furthermore, the use of small craters (e.g., <200 m) to date geographically small mare surfaces remains controversial (McEwen & Bierhaus, 2006; Williams et al., 2018). Consequently, the evidence in support of Copernican-aged mare volcanism younger than ~1.0 Ga is weak.

Recent comprehensive surveys have revealed the widespread distribution of Ring

Moat Dome Structures (RMDSs), which are lunar morphological features characterized by a relatively low, circular topography surrounded by a shallow moat. Their composition does not differ from the local mare in which they occur (their host unit) and they tend to occur in clusters in a wide range of mare settings (Zhang et al., 2017, 2018, 2020). A theoretical model of their formation (Wilson et al., 2019), based on their comprehensive characterization (Zhang et al., 2017, 2020), suggests that RMDSs represent extrusive features linked to the emplacement of the host basaltic lava flows. Accordingly, they would have formed during late-stage inflation-related emplacement processes of the flow, including second boiling, segregation of vesicle-rich magma within the flow, and its extrusion to the surface to produce the RMDS features. This model supports the contemporary formation of RMDSs and associated flows (most >3.0 Ga; Hiesinger et al., 2011). However, the superposition relationships of some RMDSs on small, degraded craters <300 m in diameter suggests a very young age, in the order of hundreds of Ma (Basilevsky et al., 2019; Zhang et al., 2020). This would place the formation of some RMDSs within the Copernican era, billions of years after the emplacement of most mare basalts. Such young ages conflict with the previous RMDS models (Wilson et al., 2019; Zhang et al., 2017).

In this contribution, we first briefly outline the nature of RMDSs and the hypothesis that suggests that they formed more than several billion years ago, contemporaneously with their host mare units, and then we present multiple lines of evidence that appear to contradict this model, and that together suggest that the

RMDS formed much later than their host lava flows, in the recent Copernican period of lunar history. We then synthesize the evidence for Copernican-aged RMDS formation and translate this into the requirements for any successful model for the generation, ascent, and eruption of magma to explain the Copernican-aged formation of RMDS. Finally, we list a series of outstanding questions and robotic/human exploration strategies that can provide definitive evidence to resolve the RMDS age conundrum and thus increase our understanding of the duration and flux of lunar volcanism and the thermal evolution of the Moon.

2. RMDS Characteristics and Distribution

Mound-like features with surrounding moats were first identified in Lunar Orbiter image data and described by Schultz and Greeley (1976) and Schultz et al. (1976) and later found in much more abundance in Lunar Reconnaissance Orbiter (LRO) image data and named ring-moat dome structures (RMDSs) (Zhang et al., 2017). Following this, Zhang et al. (2020) reported on a much more comprehensive analysis of the nature and distribution of RMDSs, summarized here. They found that the positive morphologic RMDS features occurred in clusters in many lunar mare regions, most of which had not been previously reported, and they expanded the known RMDS locations from ~2,600 to over 8,000 (yellow crosses, Figure 1). Zhang et al. (2020) presented a detailed analysis of over 500 RMDSs located in several different mare basins, combining elemental mapping, morphology and morphometry, distribution relationships, and relationships with other geologic structures. They also assessed numerous terrestrial analogs to the RMDS features. They concluded that the RMDS can be characterized as follow:

1) They are low circular mounds a few hundred meters in diameter (average ~200 m) with a mean height of 3.5 m.

2) Mounds are surrounded by moats ranging from tens to over 200 m wide and up to several meters deep.

3) They are more commonly found in moderate-to-high >3 wt% TiO_2 mare units, though a wide titanium abundance variation is observed.

4) They are found in spatial association with lava flow units and sometimes with associated volcanic-related features (e.g., Head & Wilson, 2017), such as small shields and cones (Zhang et al., 2020, their Figure 16).

5) Some but not all display some spatial associations with Irregular Mare Patches (see Braden et al., 2014), leading Zhang et al. (2020) to suggest that both may form from related lava flows.

6) Zhang et al. (2020) found a favorable comparison between lava inflationary structures on Earth and RMDSs, lending support to a hypothesis of an origin involving inflation-related extrusive volcanism and a genetic relationship of RMDSs with host lava flow emplacement processes.

7) Zhang et al. (2020) noted embayment relationships between some RMDS mounds and craters of apparent impact origin (and of different degradation states) superposed on the host mare. They concluded that these examples conflicted with

RMDS formation models in which RMDSs formed contemporaneously with their host lava flows.

Zhang et al. (2020) thus outlined two conflicting models for RMDS formation: a) Synchronous with the emplacement and cooling of their ancient host lava flows (~3–4 Ga old), and b) substantially postdating the emplacement and cooling of the host mare lava unit, likely some time during the Copernican and/or Eratosthenian periods (~0–3 Ga old).

3. The Model for Contemporaneous Host Lava Flow-RMDS Formation

This hypothesis was initially proposed by Zhang et al. (2017) and then described in detail by Wilson et al. (2019) based on a theoretical model of lava flow emplacement and cooling behavior. Wilson et al. (2019) used descriptions and preliminary interpretations of RMDSs and models of the dynamics of lunar lava flows (Head & Wilson, 2017; Wilson & Head, 2017a) to try to account for the major characteristics of RMDSs (Zhang et al., 2017, 2018, 2020). A summary of the model is as follows: in the early stages of an eruption of mare basalt, the magma contains very low quantities of dissolved volatiles and a few exsolved gas bubbles because these have been largely and efficiently lost during the pyroclastic hawaiian fire fountain activity at the vent. The lava flow surface and base cool progressively as the lava travels away from the vent, resulting in upper and lower solidified boundary layers and a molten core. Toward the end of the eruption at the vent, magma rise speed in the dike decreases as dike closure begins. This lowering of magma ascent rate enhances the ability of gas bubbles to form and coalesce, favoring strombolian activity at the vent, which removes some gas but leaves residual volatiles in solution. Magma from this phase of the eruption is then injected into the previously emplaced molten flow core causing flow inflation and resulting in substantial uplift of the flow surface. Eventually, the flow comes to a halt with the now volatile-rich inflated magma core. As the lava cools in place, it begins to crystallize, leading to supersaturation of the residual dissolved volatiles that remain in the injected flow core. This second boiling generates exsolved gas that produces massive quantities of vesicles, both at the top and bottom of the cooling central flow core. This results in the production of very vesicular to foamy layers, accompanied by further flow inflation of many meters, and causing flexing of the cooled upper crustal layer. Consequently, in turn, crustal fractures are created permitting the extrusion of magmatic foams onto the surface, driven by the buoyancy of the vesicle-rich magma. The result is the extrusion of the magmatic foam through the cracks to form the circular dome-like mounds on the surface. The extrusion is accompanied by subsidence of the surrounding surface and the solid crust below the extruded mound, in response to displacement of the foam. This subsidence is interpreted to form the ring moats surrounding the mounds.

Second boiling and inflation are commonly seen in many large basaltic flows on Earth, but RMDS formation should be facilitated on the Moon in all lava flows greater than ~50 km length and thicknesses more than ~10 m by several factors: 1) lunar basalts have low viscosity compared with terrestrial ones; 2) the predicted high effusion rates in typical lunar eruptions; and crucially, 3) the lack of a lunar atmosphere. Furthermore, the formation of extremely vesicular foams (the consequence of low lunar gravity and absence of an atmosphere), is unique to the lunar environment and permits both upward flexing and fracture of the upper thermal boundary layer surface of the lava flow, and the extrusion of the foam to form the distinctive RMDS mounds.

The RMDS emplacement model of Wilson et al. (2009) outlined above (see synthesis in their Figure 5) is characterized by numerous implications that could be formulated as hypotheses to be tested in future studies and exploration to assess, discard, or modify:

1) Shape of Domes: Foam extrusion from cracks in the uplifted summit of the underlying lava flow crust should generally lead to near circular-shaped domes. This is because the final radius of the dome is likely to be significantly greater than the linear extent of the fracture in the lava crust through which the foam is extruded; the non-Newtonian rheology of the foam, specifically its yield strength, means that its lateral spread is driven by the vertical accumulation of the bulk foam mass rather than the detailed shape of the fracture.

2) Size Variability of Individual Domes and Their Moats: The formation process of domes involves the redistribution of a volume of vesicular lava from the lava flow interior onto its surface. The material will undergo a change in its bulk density upon

emplacement, but the overall volume change and its variability should be small, and the volumes of each dome and its surrounding moat should be similar.

3) Variations in RMDS Shape: It has been shown that lava flow surface topography can vary in height by several meters over tens of meters horizontal scales (Kreslavsky et al., 2017) caused by the flow encountering earlier flows or pre-flow impact craters during its emplacement. Asymmetry in RMDS shape and alignment could be due to the intruding lava responsible for some RMDS extrusions diverting around high points or flowing preferentially into elongate topographic lows. Careful analysis of any such irregularities in RMDS clusters could lead to a better understanding of the host flow emplacement and evolution process.

4) RMDS Alignment: Patterns of linearity and alignment of individual RMDSs might be anticipated due either to fractures in distal flows caused by a) unusually extensive pre-eruption topographic variations or b) major internal magma pathways formed during late-stage inflation and second boiling. Such linear patterns should be investigated in further analysis of individual RMDS clusters.

5) Immediate Post-Emplacement Deformation of Domes: The second boiling process that leads to RMDS formation occurs in a lava flow that has come to a halt and is cooling and solidifying, and thus RMDSs are predicted not to show any deformation by shearing due to any lateral flow movement.

6) Composition/Mineralogy of Domes and Host Lava Flows: The basic composition and mineralogy of the domes and the host lava flows should be very

similar, but the domes themselves should contain a higher proportion of glass shards due to the fragmentation of the magma emerging from the surface crack at the start of dome growth.

7) Nature of Dome Material: RMDS dome material is predicted to be a basaltic lava foam characterized by a vesicularity of ~50–60%. This range is dictated by the requirement that to explain the dome morphology the foam must have a vesicularity that is large enough (>30-40%) to ensure a significant yield strength and viscosity, but is small enough (<~75%) to ensure that the foam does not disintegrate under shearing forces.

8) Initial Upper Layer of Dome Material: Dome material should be overlain by an “autoregolith”, a layer of shattered foam caused by eruption into a vacuum, composed of a mixture of loosely packed glass shards and chilled magma droplets up to a few meters-thick and with ~30% void space, the amount expected for any unwelded accumulation of irregular brittle fragments.

9) Dome Stratigraphy and Regolith Development: What is the “regolith protolith” (Head & Wilson, 2020) of the domes, the stratigraphy of the substrate immediately following their emplacement? The Wilson et al. (2019) model predicts that the regolith protolith stratigraphy will consist of an upper layer of “autoregolith” up to several meters thick, overlying a layer of very vesicular (~50–60%) foamy basalt, with this in turn overlying the upper chilled thermal boundary layer of the initially emplaced RMDS-host lava flow. There are uncertainties in both the thickness of the

extruded vesicular/foamy lava and the topography of the underlying solid basalt flow top. Wilson et al. (2019) considered two models for the topography of the underlying host basalt layer, one in which it was uplifted (favoring shedding of the extruded vesicular/foam layer and solid lava flow exposure nearer the dome summit) and one in which it subsided (favoring thickening of the vesicular/foam layer near the mound summit).

10) Predicted Nature of Post-Mound Impact Craters: Subsequent superposed impact craters should initially encounter an autoregolith layer up to several meters thick; small craters should look very similar to those in mature regolith with few to no associated boulders. Larger craters should penetrate to the vesicular/foam layer and their shape could be influenced by the amount of vesicularity; foamy lavas are predicted to behave more like an aerogel, with energy partitioning favoring crushing over ejection, with associated effects on crater depth and shape, perhaps producing narrower, dimple like structures in this part of the target substrate. Even larger craters will penetrate the uplifted (or sagged) top of the host lava flow and thus should look like normal craters superposed on the adjacent host lava flows. Careful analysis of this range of crater sizes could lead to both a testing of the hypothesis and an improved understanding of the actual emplacement processes and resulting stratigraphy.

11) Predicted Nature of Post-Moat Impact Craters: The RMDS moat marks the boundary between the extruded dome and the approximate edge of the uplifted or sagged host lava flow upper layer. Therefore, at and inside the moat, the stratigraphy

should be that of the dome, as described above. This should lie in contrast to the substrate characteristics at and outside the moat, which would be dominated by the regolith protolith of the upper solid host mare basalt layer. Impact craters that are superposed on the RMDS boundary are predicted to reflect these differences in RMDS and host-basalt substrates. The portion of the superposed crater in the host-basalt substrate should appear similar to a normal mare basalt regolith crater, but the portion of the superposed crater in the dome material should be much less distinct, with a poorly formed rim crest and ejecta deposit due to the unusual nature of the initial autoregolith and extruded vesicular/foam layer. These contrasting characteristics should be further enhanced by the potential downslope movement of fragmental dome material due to the somewhat steeper slopes of the dome flanks.

12) Predicted Differences Between Post-RMDS and Post-Host Mare Basalt Flow Impact Craters: Potentially, the morphology and morphometry of impact craters superposed on the host mare basalt substrate and the domes could be used as a first-order test of the Wilson et al. (2019) extruded vesicular/foam layer hypothesis for the origin of RMDSs. This test is made more difficult, however, by the complex mode of emplacement and autoregolith formation, as well as the uncertainty in the uplift and sagging of the host basalt surface underlying the domes. Very careful analysis of these superposed craters based on the criteria outlined above can serve to test the hypothesis further and even potentially derive an improved understanding of the model uncertainties.

13) Further Tests of the Flow Inflation/Second Boiling RMDS Model: A characteristic of the Wilson et al. (2019) extruded vesicular/foam layer hypothesis for the origin of RMDSs is that the host flow substrate consists of a highly vesicular lava flow core underlying the upper cooled layer of the mare basalt flow, and that the deformation of this layer led to the extrusion of parts of this core to produce the RMDSs. Implicit in this interpretation is the fact that the interior of the flow could have a very high micro- and macro-porosity remaining upon cooling and solidification, thus consisting of potential void spaces, particularly where the solid basalt layer has been fractured and tilted and the magma below the upper layer has been extruded. In a somewhat analogous case of a small shield volcano late-stage summit crater evolution at Ina, Qiao et al. (2019) and Wilson et al. (2019) have called upon such macroporosity to enhance regolith drainage into the underlining voids to explain similar mound-moat relationships.

However, detailed mapping of the relationship of RMDSs to the host mare basalt substrate has revealed examples where individual RMDSs appear to embay circular depressions in the host substrate (Basilevsky et al., 2019). The superposition of RMDSs over craters (RMDS-crater-overlap) suggests that the specific crater-embaying RMDSs may be younger than both the mare substrate and the crater, pointing to an extended time (of unknown duration) that might have occurred between the host mare basalt substrate emplacement and the formation of the domes. This study thus aims to use both morphometric analysis and a topographic diffusion model to date some small craters (100-300 m in scale) which are partially overlapped by RMDSs (Figures 2 and 3). Our results show that the emplacement of this RMDS-related volcanism may have occurred up to several hundreds of millions of years ago (i.e., 130-1500 Ma), thus challenging the present consensus on the thermal evolution model of the Moon, which places an upper limit for the cessation of mare volcanism at ~2.0 Ga ago (e.g., Spohn et al., 2001; Ziethe et al., 2009).

4. Data and Methods

The high-resolution Lunar Reconnaissance Orbiter Camera (LROC) NAC images (Robinson et al., 2010) at 0.42-1.5 m/px (to date the highest spatial resolution available from lunar orbit), and 2 m/px NAC-based DTMs constructed using shading method (see the detail by Zhang et al. (2020) and references therein) were used in this study. All the raw and calibrated NAC image data are accessible via the NASA Planetary Data System (PDS), and calibrated and projected using the USGS ISIS software. These images were then investigated using the software ArcGIS 10.6. We relied on the comprehensive analysis of the distribution and characterization of RMDSs as outlined in Zhang et al. (2020).

4.1 Age Estimation from Crater Morphometry

The ages of the craters superposed by RMDSs, which are relatively younger, can be estimated based on crater morphology, morphometry, and size relations (Basilevsky, 1976). The RMDS heights (h), height/diameter ratios (h/D) and maximum steepness of their slopes (β), as well as the crater depths (d), depth/diameter ratios (d/D) and maximum steepness of inner slopes (α) were measured from NAC-based DTMs. For impact craters, these parameters allow us to approximately estimate their absolute ages (Basilevsky et al., 2019) and thus evaluate if the RMDSs formed during the time of the basaltic plains infill or later.

4.2 Age Estimation from a Topographic Diffusion Model

Another method that can be used to constrain the age of a lunar crater is to determine its degradation state by using a topographic diffusion model. Fassett and Thomson (2014) determined the degradation state of about 13,000 lunar craters on the lunar maria, implicitly assuming that the diffusivity was independent of crater size. Linking their measurements of the degradation states to surface ages, they derived a relationship between degradation state and crater age. More recent work, however, showed that diffusivity varies with crater diameter (Fassett et al., 2018; Xie et al., 2017). Considering this updated crater size-dependent topographic degradation of lunar craters, Fassett et al. (2018) revised the relation of Fassett and Thomson (2014) as:

$$K_{1000\,m}(t) = 363.58t^5 - 2954t^4 + 8953t^3 - 13814t^2 + 16695t \qquad (1)$$

where K_{1000m} is the diffusion age of a crater with a diameter of 1000 m which is defined as the product of diffusivity and time (Fassett & Thomson, 2014), and t is time in Ga. The model of Xie et al. (2017) gives the relation between K_{1000m} and the diffusion age of a crater with an original diameter of D_0:

$$K_{1000m} = \left(\frac{1000}{D_0}\right)^{0.93} K(D_0) \quad (2)$$

To determine the diffusion age of each RMDS-superposed crater, we used the approach of Fassett and Thomson (2014) as follows: first, the profile of a RMDS-embayed crater was derived from a detrended DTM (which is the difference from the DTM to the pre-impact surface). The pre-impact surface is constructed by fitting a plane to the elevation data beyond 1.5 radii from the crater center. The regions used for the extraction of topography are shown as blue polygons in Supplementary Figure S1. Second, a database of crater profiles in various degradation states was derived from the topographic diffusion model for D = 50 m to 400 m craters using the initial crater profile model of Xie et al. (2017). Finally, we found the profile from the database that best matches the profile of each RMDS-embayed crater derived in the first step. The best-fitting profile provides estimates of the original diameter (D_0) and the diffusion age ($K(D_0)$) of an observed crater. By using Equation (2), we derived K_{1000m} from the $K(D_0)$, and then by solving Equation (1) we obtained the estimated age of the crater.

4.3 Age Estimation from Using a Locally Calibrated Monte Carlo Model

The diffusion rates taken from the literature and used in the previous sections (see Section 4.2) to estimate the ages of the small impact craters overlapped by RMDSs were all derived from global considerations. Furthermore, a general expression for the dependence of the diffusion rate κ on the crater diameter D has not been established yet. Hence, we assumed a dependence in the form of a power law

$\kappa = b\ D^{a}$ (Fassett et al., 2018) and determined the parameters a and b based on the cumulative size-frequency distribution (CSFD) of an area located close to the RMDS-overlapped crater. The Monte-Carlo cratering model introduced by Bugiolacchi and Wöhler (2020) was then adapted to the observed CSFD, thus yielding the parameters a and b for the region under study. In turn, these locally calibrated parameters allow for an estimation of the ages of craters overlapped by RMDSs.

For counting the craters, we build upon the deep-learning-based automatic detection algorithm introduced by Wilhelm and Wöhler (2021). The original method relies on a convolutional neural network (CNN) that is applied to windows of variable size extracted from an LROC NAC image. In this study, however, to achieve robustness concerning variable illumination conditions, we trained the CNN to high-resolution LROC NAC DEM data obtained by shape from shading (Grumpe & Wöhler, 2014; Grumpe et al., 2016; Zhang et al., 2020). The training data for the CNN were extracted from the DEM using the manual crater annotations by Fisher (2014), consisting of a set of 852 crater locations with diameters between 5 and 41 m, determined based on a LROC NAC image. The LROC NAC DEMs presented by Zhang et al. (2020) have a pixel size of 2 m. As the technique of Wilhelm and Wöhler (2021) is specifically favorable for detecting small craters of about 5-10 pixels size, the LROC NAC DEM under study was presented to the CNN in 23 down-sampled resolution levels covering a factor of 12, so that all craters between 10 and 100 m diameter were detected with virtually the same probability. Since most craters are detected several times on different resolution levels with slightly different estimated center positions and/or diameters, a clustering stage is used to aggregate multiple detections of the same crater. For further details about the algorithm see Wilhelm and Wöhler (2021). The automatic crater counts were then used to construct the CSFD of the examined region in the crater diameter interval of 10-100 m.

To obtain parameters *a* and *b*, we used the Monte-Carlo cratering model of Bugiolacchi and Wöhler (2020). This model simulates the population of small craters with diameters between 10 and 100 m over time by adopting the cratering rate and production function of Neukum et al. (2001), where the number of craters per diameter interval is modeled by a Poisson distribution whose mean is defined by the production function. Given the values of *a* and *b*, a diffusion rate and thus a lifetime can be assigned to each crater according to its diameter. Based on Fassett et al. (2014) it is straightforward to show that the crater lifetime T_{life} is given by

$$T_{\mathrm{life}} = \frac{T_{\mathrm{life}}^{(0)} \kappa_0}{D_0^2 b} D^{2-a} \tag{3}$$

with $T_{\mathrm{life}}^{(0)}$ as the lifetime of a crater with diameter D_0 for a diffusion rate κ_0, where D_0 and D are given in km. Assuming that the lifetime of a crater is reached once its depth has fallen below 1% of its initial diameter, we found by numerical integration of the standard diffusion equation (e.g., Fassett & Thomson, 2014) that for a crater with $D_0 = 0.3$ km and $\kappa_0 = 7\ \mathrm{m}^2/\mathrm{Ma}$ it is $T_{\mathrm{life}}^{(0)} = 3.07$ Ga, assuming the initial cross-sectional crater profile proposed by Fassett et al. (2014). The factor $\frac{T_{\mathrm{life}}^{(0)} \kappa_0}{D_0^2}$ in equation (3) is a dimensionless normalization constant whose value is 0.239, independent of the chosen values of κ_0 and D_0. The diffusion equation determines that the value of $T_{\mathrm{life}}^{(0)}$ is proportional to D_0^2 and to $1/\kappa_0$, so that the value of the normalization constant does not change upon variations of κ_0 and D_0.

At each time step of the simulation, it is checked for each crater if its age exceeds its lifetime; if this is the case, the crater is marked as invisible. Other mechanisms to make a crater disappear are destruction by a new larger crater and covering of the crater by the ejecta of a new larger crater. In our simulations, we found that these mechanisms are 2-3 orders of magnitude less efficient than diffusion for the diffusion rates inferred for our three regions under study (see Table 1). Our model also takes into account the gradual increase of the crater diameter over time (Bugiolacchi & Wöhler, 2020; Xie et al., 2017). At any desired time step, a CSFD can be extracted from the simulated crater population. For the crater diameter interval of 10-100 m, we found for any reasonable choice of *a* and *b* that yields values for the diffusion rate comparable to the literature (e.g., Fassett et al., 2014) that the CSFD converges into an equilibrium state after at most 100 Ma.

Because of the Monte Carlo nature of our model, the simulated CSFD at a specific moment in time is different for each simulation run. It is thus not possible to fit the cratering model to the observed CSFD with standard, e.g., gradient-based, optimization techniques due to the statistical fluctuations of the error function. Hence, we perform the fitting of the model parameters using a Bayesian optimization technique (e.g., Gelman et al., 2013; Snoek et al., 2012), which is able to cope with a non-deterministic error function. We chose the sum-of-squares deviation between the measured and modeled logarithmic CSFD values as the error function and optimized the logarithms of two diffusion rates κ_{10} and κ_{100} for craters of 0.01 km and 0.1 km diameter, respectively, which are related to the parameters *a* and *b* by $a = \log_{10}(\kappa_{100}/\kappa_{10})$ and $b = 10^{a+\log_{10}\kappa_{100}}$. The obtained values of κ_{10} and κ_{100} are listed in Table 1. For all three examined regions located close to the RMDS-overlapped craters shown in Figures 2a-2c, respectively, the smallest 2-3 diameter intervals are excluded from the fit because they are already influenced by the rollover effect, i.e., an artificial flattening of the CSFD due to incomplete detection of the smallest craters.

Apart from computing the lifetime of the RMDS-overlapped craters, the values of *a* and *b* found by the Bayesian optimization routine also allow for estimating the actual age of these craters, given their diameters and depths. These dimensions correspond to 0.3 km / 15 m for the RMDS-overlapped crater-containing areas (Figures 2a and 2c) and 0.13 km / 4 m for the area close to the case shown in Figure 2b. Using the initial cross-sectional crater profile of Fassett and Thomson (2014) and a diffusion rate of $\kappa_0 = 7\ \mathrm{m}^2/\mathrm{Ma}$, we found that a crater of diameter $D_0 = 0.3$ km needs a time of $T^{(0)} = 630$ Ma and 1040 Ma, respectively, until it reaches these depth/diameter ratios. Since the time needed by a crater to reach a certain degradation state is proportional to the squared diameter D^2 and inversely proportional to the diffusion rate κ, the crater age T is then given by:

$$T = \frac{T^{(0)}\kappa_0}{D_0^2 b} D^{2-a} \tag{4}$$

5. Results

5.1 RMDS-Impact Crater Embayment Relations

The RMDS-crater-overlap examples (red stars, Figure 1; see also other candidate cases in Supplementary Figure S2) were identified from spectrally defined mare units older than 2.0 billion years based on crater size-frequency distribution (CSFD) measurements (Hiesinger et al., 2006; 2011). The features in Figures 2a-2d are in Maria Tranquillitatis, Humorum, Fecunditatis, and Tranquillitatis, respectively, corresponding to the mare units T26 (3.46 Ga), H6 (3.46/3.75 Ga), F7 (3.34/3.62 Ga), and T18 (3.62 Ga) defined by Hiesinger et al. (2006, 2011). The two cases in Figures 2e and 2f are in Imbrium mare unit I30 (2.01 Ga). Clearly, if RMDSs had formed concurrently with the emplacement of these mare lava flows, they would have ages comparable to those of their hosting mare units, i.e., > 2.0 Ga (Supplementary Figure S3). Therefore, these embayment relationships alone would contradict the hypothesis of synchronous formation of the mare basalt host unit and the associated RMDSs (Wilson et al., 2019; Zhang et al, 2017, 2020; see Section 3 for more details).

5.2 Degradation Ages of Impact Craters Embayed by RMDSs

Morphologic and morphometric characteristics suggest Copernican-aged (<1000 Ma) basaltic mare volcanism associated with RMDSs. Figure 2 presents six cases when RMDSs appear to be superposed on adjacent craters. A three-dimensional rendering based on NAC-derived DTMs is shown in Figure 3. NAC DTM-based topographic profiles extracted along the lines cutting across these craters and the RMDSs can be found in our supplementary Figures S4-S9. The statistical results obtained according to the topographic information are listed in Table 2. The D and d of both craters superposed by RMDSs in Figures 2a and 2c are ~300 m and ~15 m respectively, resulting in a d/D ~0.05 with a maximum steepness of the inner slope, α, of ~9°. This type of crater belongs to the morphologic class C defined by Basilevsky (1976), corresponding to an age between 750 and 1500 Ma (Figure 4 and Table 2).

The crater in Figure 2b is ~130 m in diameter with a shallow depth of 4 m, d/D of 0.031 and α about 6-8°. Its estimated age appears to be in the range of ~160-320 Ma. Figure 2d shows a RMDS of a size of 140 x 160 m and a height of 1-1.5 m, overlapping a 140 m crater. This RMDS-superposed crater has d ~7-9 m, d/D = 0.04-0.06, and a maximum inner slope angle of 8-9°. It is classified as a type C crater in its intermediate phase of destruction (Basilevsky, 1976), thus giving an age of around 200-300 Ma and, consequently, requiring an even younger age for the superposed RMDS. Therefore, the RMDSs that superposed these craters should be younger than these age values, thence, the crater ages provide a *maximum* age for the RMDS emplacement events.

The RMDS in Figure 2e is 2-3 m tall, ~170 m across and superposed on a crater with D ~100 m. Its slopes are 2-3° to 8-10° (at the contact with the crater). The embayed crater has a depth (d) of 5-6 m with a range of d/D values of 0.05-0.06, and its inner slopes are up to 8-10° steep. Morphologically, it belongs to the crater of class

C (Basilevsky, 1976; Figure 4) in the first half of its life, corresponding to an age of 200-300 Ma.

The RMDS in Figure 2f is characterized by an elliptical shape in plain view, with a dimension of 230 x 280 m, and the diameter D of the crater superposed by the RMDS is ~135 m. The RMDS is only ~2 m high and its slopes just up to 3-4° steep. The depth of the crater is ~5-7 m, and so the ratio d/D > 0.04. The maximum inner slope angle of the crater is ~7-8°. It belongs to craters of class C and its age is ~200-300 Ma (Figure 4 and Table 2), and thus, the age of the embaying RMDS should be < 200-300 Ma.

5.3 Diffusion Model Ages for Impact Craters Embayed by RMDSs

Based on a topographic diffusion model (Fassett & Thomson, 2014; Xie et al., 2017), degradation states for the six craters of different sizes which are embayed by RMDSs to varying degrees, were derived using ~2 m/pixel NAC DTMs. Their crater topography (Supplementary Figure S10) and model fits results are shown in Figure 5 and Table 2. The ages of RMDS-embayed craters range from 130 to 1000 Ma. There is a positive correlation between the ages and diameters of these craters superposed by RMDSs, possibly because smaller craters preferentially sample younger ages, as the lifetime of craters increases with size (Xie et al., 2017). These findings provide additional support for a younger age of RMDS emplacement (Figure 4), uncoupled from the surrounding mare infill events.

5.4 Simulation Results from Using a Locally Calibrated Monte Carlo Model

Simulation results for the RMDS-impact crater embayment areas (Figures 2a-2c) obtained with the median values of κ_{10} and κ_{100} are shown in comparison with the observed CSFDs in Figure 6. The distributions of the resulting lifetimes and ages of the RMDS-overlapped craters in the three areas (i.e., areas located close to the RMDS-overlapped craters in Figures 2a-2c, respectively) are shown as boxplots in Figure 7. The inferred median ages of the RMDS-overlapped craters are all younger than 200 Ma, and the upper marginal values of the distributions are below 500 Ma. These crater age values are upper limits to the ages of the overlapping RMDSs, again providing additional evidence for favoring the young age (i.e., Copernican in age, <1.1 Ga) of RMDS-formation-related mare volcanism.

6. Discussion

The detailed hypothesis for RMDS formation concurrent with the host lava flow (e.g., Wilson et al., 2019) has been described in Section 3. We now outline in more detail: 1) the list of observations that conflict with the prediction of the concurrent RMDS-host lava flow formation; and 2) a set of observations that any hypothesis for the young origin of RMDSs relative to their host basalt unit must address. We conclude with a set of research and human/robotic mission goals and objectives that could help to resolve the age conundrum for the formation of RMDSs.

6.1 Contradictions to Predictions of the Contemporaneous Host-Lava Flow-RMDS Formation Model

Several observations contradict the predictions of the Wilson et al. (2019) model of the contemporaneous formation of the host lava flows and RMDSs. Examination of the relation between RMDSs (diameters in the range of hundreds of meters) and impact craters of about the same size and smaller shows that numerous case studies selected from a large population pool of more than 8,000 RMDSs (Figure 1; Zhang et al. 2020) support the occurrence of eruptive volcanism on the Moon much younger than proposed by the model. Additionally, as estimated by Fassett and Thomson (2014) and others, the smaller-than-300 m crater retention ages for the Moon are consistent with ages substantially younger than 3.0 Ga. Furthermore, according to the current understanding of small lunar crater degradation rates based on diffusivity models (e.g., Fassett & Thomson, 2014; Xie et al., 2017), some craters embayed by RMDSs are so small (even less than ~150 m diameter, Figure 2 and Supplementary Figure S2 for other candidate examples) that they could not have survived for 3 Ga. Based on the NAC-derived digital terrain models (DTMs, Grumpe & Wöhler, 2014; Grumpe et al., 2016), the model ages of RMDS-superposed small craters can be inferred from topographic measurements (Basilevsky, 1976) and a topographical diffusion model (Xie et al., 2017). However, given the widespread distribution of the RMDSs across lunar mare surfaces, these potential younger ages have implications that would revolutionize our models of the thermal history of the Moon (Shearer et al., 2006). We also explored morphologically similar endogenetic crater features occurring in terrestrial basaltic lava flow fields and cannot rule these out, but even if the features embayed were not typical impact craters, the required billions of years lifetime of such small depressions appear unlikely. We now turn to several lines of evidence and additional related factors, and address them individually.

6.1.1 RMDS-Impact Crater Embayment Relations

Could the examples of identified RMDS-embayed craters (e.g., Basilevsky et al., 2019; Figures 2 and 3) have formed during host lava flow emplacement (for example, after the emplacement of the flow but before its final inflation, cooling, second boiling, volatile release and RMDS eruption)? Wilson et al. (2019) estimate that the duration of flow emplacement and solidification is of the order of less than several years, and thus it is: 1) highly improbable that an individual superposed impact crater would form during this extremely short period (even in a period of relatively higher flux; Stöffler et al., 2006); and 2) also highly improbable that such an impact crater would survive over three billion years of subsequent regolith development.

Could the RMDS-embayed craters be contemporaneous with flow emplacement and be of endogenetic origin? Inflation features in terrestrial basaltic lava flow fields provide clues as to the mode of formation of crater-like depressions. Some endogenetic surface depressions represent circular lava-rise (or inflation) pits (Figure 8) formed by the vertical inflation of the host lava flow around local topographic highs on the pre-flow surface, leaving a depression (e.g., Hamilton et al., 2020; Walker, 1991). In other cases on Earth, lava mounds, all high areas within a lava field, are sometimes locations for the formation of small drained sub-lava-crustal lava caves (Grimes, 2002), whatever the process of mound formation.

In addition, in the RMDS contemporaneous formation model, the RMDSs could collapse due to the removal of the pressure or withdrawal of melt that caused their eruption. An array of circular to irregular-shaped collapses or depressions associated with RMDSs has been observed during our investigations (Zhang et al., 2017, 2020). This could also be comparable to a range of variation among tumuli displaying summit cracks and various types of collapse (e.g., Ollier, 1964; Walker, 1991).

Terrestrial basaltic lava flow fields emplaced by inflation commonly display depressions of variable shapes. For example, the Aden flows, located in south-central New Mexico, covering an area of ~75 km^2 consist of thin vesicular flows (De Hon & Earl, 2018; Hoffer, 1976). The Aden inflated flows are pock-marked with inflation pits 20 to 150 m across and 4 to 5 m deep (Figure 8). They are characterized by gentle interior slopes caused by the continuous extensional collapse of the marginal crust. In some areas, molten rock withdrew from subterranean spaces (such as drained lava tubes), leaving voids into which the surface collapsed, forming a series of collapse pits/depressions.

On Earth, dimple-shaped drainage craters (Greeley, 1970) and raised-rim collapse craters (Greeley & Gault, 1979) were found in basaltic lava flows and interpreted as endogenic morphologies formed in association with lava tubes. However, previous studies (e.g., Greeley & Gault, 1979) often misinterpreted lava-rise or inflation pits (Walker, 1991) as collapse depressions. Impact crater-like profiles are expressed through several inflation pits (e.g., Figure 8). Nevertheless, whether their formation was related to lava tubes or not, collapsed craters should also exist on the Moon and other planetary surfaces where basaltic volcanism has once occurred and have an appearance practically indistinguishable from small impact craters (e.g., 100 m or smaller). Collapse crater size is mostly governed by the lava flow thickness (e.g., Greeley & Gault, 1979) and subsurface tube dimensions. Lunar basaltic lavas are more fluid than the terrestrial equivalent (Williams et al., 2000), and more collapse craters tend to form in these, relative to more viscous flows (Greeley & Gault, 1971).

Terrestrial inflation and collapse pits appear to be most frequent on inflation plateaus, whereas circular mound-like positive features are also found to coexist with these negative features. An inflation plateau (Figure 8) represents a topographically flat-topped uplift resulting from a kind of uniform “inflation” by injection of lava beneath a rigid upper crust (Hon et al., 1994; Walker, 1991; Wentworth & Macdonald, 1953). During the repeated inflation process (Self et al., 1998; Wilson et al., 2019), interior hot lava can reach the surface via cracks in the flexing lava crust which formed when the interior pressure exceeds the tensile strength of the overlying cooled flow layer. Crater-like forms and circular tumulus-like structures (yellow and white arrows in Figure 9) on inflation plateaus in the Amboy lava flow field, Mojave Desert, California, reveal various inflation-caused positive and negative features formed during flow emplacement. Some tumulus-like structures show degraded appearances to varying degrees (red arrows, Figure 9). Among these, one shows a central collapse pit filled with sand/dust deposits (the upper red arrow, Figure 9), while the lower one has evolved into a circular collapse depression with a broken, blocky rim (the lower red arrow, Figure 9). These circular negative and positive features on the inflationary lava flow surface provide potentially good analogs for RMDS and crater formation that are very likely to have occurred in basaltic lava flows on the Moon. A better description of the nature of such negative and positive features, both of which are endogenic in origin, is of geologic importance for the full understanding of inflationary features that might have occurred on the Moon, and that might have produced essentially simultaneous circular endogenetic surface depressions into which near-contemporaneous RMDSs might have flowed. Thus, simultaneous endogenetic depressions cannot be ruled out as a candidate to explain the RMDSs-superposed crater-depression embayment relationships (e.g., Figures 2-3 and Supplementary Figure S2).

In addition, the RMDS-superposed depressions have impact crater-like raised rims, similar to those of terrestrial collapsed tumuli with broken and blocky raised rims (De Hon & Earl, 2018; Ollier, 1964). This also allows the possibility that RMDS-superposed craters might be of non-impact origin. Lunar craters that are partially superposed by RMDSs have more gentle interior slopes (commonly < 10°, Section 5.2). The Aden basalt is very young (middle to late Quaternary) with a surface-exposure age of only about 0.2 Ma (Anthony & Poths, 1992); thus, the comparison with the RMDSs-laden flows of hundreds of millions or even billion years ago on the Moon cannot be straightforward. There should be a strong negative correlation between the crater interior slopes and their longevity due to the formation and dynamics of lunar regolith and the fact that lunar topography evolves with time (e.g., Basilevsky, 1976; Fassett et al., 2014). However, if this assumption (i.e., these RMDS-embaying craters were of collapse in origin) is proven to be correct, then the question remains as to how such small craters could have survived billions of years of regolith development on the Moon if the RMDSs had formed concurrently with their host maria (Zhang et al., 2017, 2020; Wilson et al., 2019). We address this question in the following section.

Could the RMDS-embayed craters be some sort of *post-RMDS impact event*, with land sliding and mass wasting then occurring to produce an *apparent embayment relationship*? For example, could the RMDS-overlapped craters (Figure 2) have formed *after* the RMDSs? In this scenario, the crater formation event might have triggered landslides of RMDS materials into the craters, creating an *apparent* embayment relationship, thus weakening the hypothesis of a late-stage formation of the RMDS. However, the very gentle slopes (a few degrees only) typical of the RMDSs are probably not steep enough to trigger landsliding. Nonetheless, an improved understanding of how post-impact-crater formation mass wasting could modify and shape the RMDS-associated morphologies is necessary to fully address this relationship. Mass wasting and the possible role it played in shaping RMDS-hosting lava flow morphology in inflated mare regions is an important topic that needs more research.

In summary, stratigraphic relationships show multiple examples of RMDSs that clearly appear to be stratigraphically superposed on circular depressions (Figures 2-3 and Supplementary Figure S2), and, consequently, to have formed later. Based on flow cooling and solidification time, such depressions are unlikely to be of impact origin that occurred simultaneously with flow emplacement. Endogenetic craters that form simultaneously with the host lava flow are well-known in terrestrial lava flow fields and cannot be ruled out as a contributing factor to these RMDS-crater embayment examples. Taken together, however, these crater embayment relationships strongly suggest that RMDS formation did not occur simultaneously with host lava flow emplacement, thus apparently invalidating the hypothesis (Wilson et al., 2019) of flow inflation and second boiling for contemporaneous emplacement of the host lava flow and extruded RMDSs. Having assessed the *relative ages* of these RMDS-embayed crater examples, we now turn to an analysis of the morphology and morphometry of the embayed craters to assess their *absolute ages* and to estimate the *amount* of time between host lava flow emplacement and emplacement of the superposed RMDSs.

6.1.2 Degradation Age of Impact Craters Embayed by RMDSs from Morphometric Analysis

A summary of the crater-degradation age dating results (see Section 5.2) and their implications for the maximum ages of the superposed RMDSs that embay them is shown in Figure 4 and Table 2. The craters, which are interpreted to be of impact origin and to have undergone typical degradation rates since their formation

(Basilevsky, 1976), have *maximum* ages of hundreds of millions of years. Thus they are likely to have formed in the Copernican Period, significantly post-dating the formation of the mare basalt host units, and raising questions on the hypothesis for the simultaneous formation of RMDSs and their host mare basalt unit (e.g., Wilson et al., 2019).

6.1.3 Lateral Diffusion and Erasure of Small-Scale Topography: Age Estimation from Topographic Diffusion Models

Based on a topographic diffusion model (Fassett & Thomson, 2014; Xie et al., 2017), the degradation states for the six craters of different sizes (Figures 2a-2f) which are embayed by RMDSs to varying degrees, were derived using ~2 m/pixel NAC DTMs. Their crater topography (Supplementary Figures S4-S9) and model fit results are shown in Figure 5 and Table 2. The ages of RMDS-embayed craters range from 130 to 1000 Ma. Analysis of crater equilibrium suggests that a period of 1.65 Ga (the absolute model age of northern Sinus Medii; Xie et al., 2017) would be sufficient to ensure that craters smaller than 200 m would be degraded beyond recognition (Xiao & Werner, 2015). Some craters overlapped by RMDSs are so small (even less than ~150 m diameter, Figures 2e and 2f) that they cannot have retained their morphologies for up to 3 Ga, the young age of the majority (peak temporal occurrence) of the maria (Hiesinger et al., 2011) in which the RMDSs are found. The crater degradation models predicted that the maximum lifetime of a D = 150 m lunar crater was ~800 Ma (Fassett &Thomson, 2014). These results provide additional support for a younger age of less than 1.0 Ga for these RMDSs.

6.1.4 Age of Impact Craters Embayed by RMDSs from a Locally Calibrated Monte Carlo Model

The diffusion rates used in Section 6.1.3 to estimate the ages of the small impact craters overlapped by RMDSs were derived from global considerations. The Monte-Carlo cratering model introduced by Bugiolacchi and Wöhler (2020) treats the age estimation of craters overlapped by RMDSs locally. The modeling results for the RMDS-impact crater embayment areas (Figures 2a-2c) show that the inferred median ages of the RMDS-overlapped craters are all younger than 200 Ma and the upper marginal values of the distributions are below 500 Ma (Figure 7). These crater age values are upper limits to those of the overlapping RMDSs, given further support to the young age of the RMDS emplacement hypothesis.

6.1.5 Age of RMDSs Inferred from Regolith Thickness Development Models

In addressing the problem of the formation age of RMDSs, it is worth considering the effect of regolith-forming impact gardening, which influences the entire exposed lunar surface (McKay et al., 1991). Despite their modest height (~3.5 m on average for the measured 532 RMDSs; Zhang et al., 2020) and gentleness of their slopes (summit slope <5°and marginal slope up to 10°, Zhang et al., 2020), RMDSs in images with relatively low sun-illumination angle look distinct, with well-defined outlines.

A key observation is that RMDSs do not show a sequence of morphologic degradation, as do craters formed on mare surfaces over a long time. Instead, individual RMDSs, RMDS chains, and RMDS clusters formed on host basaltic units of a variety of ages (Hiesinger et al., 2011) are characterized by comparable morphologic sharpness and crispness. For example, nearly all the RMDSs highlighted in this study are located within mare lava plains with absolute model ages of 3.2-3.6 Ga, estimated by the spatial densities and size-frequency distributions of superposed craters (e.g., Hiesinger et al., 2011; Morota et al., 2011). How can RMDSs formed simultaneously with their ancient host units retain this comparable crispness if the original units are of different ages and if superposed craters, comparable in scale to RMDSs, are undergoing constant micrometeorite bombardment, degradation, and destruction?

Regolith is created by impact gardening of the lunar surface (Shoemaker et al., 1969) and its mean thickness in maria is estimated to be about 4-5 m (e.g., Bart et al., 2011; Basilevsky, 1974; McKay et al., 1991; Shkuratov & Bondarenko, 2001). The process of regolith formation encompasses two interrelated issues: 1) craters are excavated at the impact point by penetration through the regolith into underlying basaltic regolith protolith (e.g., Head & Wilson, 2020), resulting in an increase in the thickness of the regolith in any given region; 2) ejecta from these craters form regolith-like material, which is thicker closer to the crater and progressively thinner with distance. Although a minimal part of the ejecta is ballistically transported to great distances (kilometers and tens of kilometers), a significant part of the ejecta is deposited near the point of impact from a few tens to a few hundred meters depending on the size and velocity of the impactor. This scenario was supported by observations of the thinning of the regolith layer in the rim crest region of relatively large linear depressions (Rima Hadley – Apollo 15; Fossa Recta – Lunokhod 2) where ejecta from small craters are scattered in all directions but the adjacent depression is effectively a zone of negative balance of ejected material (Basilevsky et al., 1977; Swann et al., 1972).

The lunar maria with an average age of ~3.5 Ga (Hiesinger et al., 2011) have since been reworked to a depth of 4-5 m, thus destroying pre-existing features of this height (as most of RMSDs are). Larger features had their topographic relief reduced and were smoothed with a loss of morphological sharpness. RMDSs could have developed their present characteristics in the last 1 Ga only if the cumulative cratering flux had been an order of magnitude smaller in the last 3.5 Ga (e.g., Hartmann et al., 2007, their Figure 4). The ejecta excavated from small craters close to the areas surrounding any RMDS would have had a strong influence on the original morphology of RMDSs. Thus, these relationships and factors seem to require that RMDSs should have been very significantly modified or even destroyed if they had formed coincident with peak mare volcanic activity ~3.0-3.7 Ga ago. Regolith development principles would predict that RMDS marginal steep slopes and surrounding ring moats would be locations most sensitive to this type of destruction. Given that many RMDSs, including the cases reported in this study, share a well-preserved morphology (Zhang et al., 2020), we are led to conclude based on regolith development models that any RMDS formed on host-mare basalt units in these ancient times would have been degraded and obliterated in the ensuing period of regolith development: consequently, the RMDSs seen in association with these ancient host units were not formed synchronously with these units but must, instead, be relatively young, of Copernican age (from ~1100 Ma to present).

6.1.6 Density Distribution of Superposed Impact Craters

The size-frequency distributions of superposed impact craters on the RMDS-hosting mare units have been used to estimate the Absolute Model Ages (AMAs) of these units (e.g., Hiesinger et al., 2011) and these hosting units are predominantly more than ~3 Ga in age, as described above. However, if the evidence points to a much younger age for the specific examples that embay degraded craters, and regolith and diffusional degradation modelling favor a Copernican age for *all* RMDSs, what then are the AMAs of the RMDSs themselves?

Unfortunately, individual RMDSs are too small (average diameter ~200 m) to be dated reliably (e.g., van der Bogert et al., 2015). One approach would be to count superposed craters on RMDSs occurring in large clusters to build up sufficiently robust statistics to make the counts reliable, but such analyses have not yet been undertaken.

If RMDSs represented a specific facies of lunar mare basaltic volcanism it would be logical to expect that they formed between 3.9 to 3.3 Ga (e.g., Head & Wilson, 2017); this agrees with estimates (Zhang et al., 2017) from counts of craters ≥300 m on a 60 km^2 area containing both RMDSs and adjacent mare surfaces. The absolute model age (AMA) of this "mixture" was estimated to be 3.2 + 0.2/-0.7 Ga, although this figure was based on counts of only 12 craters. Therefore, counts of smaller craters were also involved (Zhang et al., 2017): producing AMAs of 25 ± 2 Ma for the RMDSs and 36 ± 0.5 Ma for the adjacent mare. However, using small, sub-km diameter impact craters to date very young planetary surfaces is not a scientifically robust methodology, given that their lifespan and distribution are more susceptible to varying degrees of degradation over geological times (Williams et al., 2018). Consequently, the distribution of craters smaller than 300-500 m can be assumed to be in equilibrium, i.e., the crater size-frequency distribution (CSFD) is less steep (slope approximately -2) and lies well below the CSFD predicted by the "de-facto standard" Neukum et al. (2001) model (see, e.g., the CSFD of the planned Chandrayaan-2 landing site shown by Sinha et al., 2020; see also Xiao and Werner, 2015). Nonetheless, the difference was explained by Zhang et al. (2017) as being due to "several physical factors related to the target's properties, such as porosity, the thickness of the regolith, the angle of slope, etc., affecting the rate of degradation". The major question, however, remains the alleged very young age. One possibility considered was that they represent "geologically very recent small eruptions occurring several billion years after the emplacement of the mare lava flows" (Zhang et al., 2020). A second scenario considered was that RMDSs are formed from magmatic foams below a cooling lava flow surface and extruded to produce the domes above the solid basaltic flow top as the flow evolved (Wilson & Head, 2017b). Impacts into foamy materials should produce smaller and deeper craters (Wilson & Head, 2017b) that may explain the unusually low AMA. However, as shown by Basilevsky and Michael (2021), impact craters superposed on the analogous mounds in the Ina small-shield pit crater (Qiao et al., 2019) appear similar in morphology to those in the surrounding maria.

6.1.7 Morphologic Characteristics of Impact Craters Superposed on RMDSs

Basilevsky et al. (2019) considered the scenario in which RMDSs are formed from magmatic foams below a cooling lava flow surface and extruded to produce the domes above the solid basaltic flow top as the flow evolves (e.g., Wilson et al., 2019). The model predicts that impacts superposed on foamy materials should produce smaller and deeper craters and this was suggested to potentially explain the unusually low AMA described in Zhang et al. (2017). Basilevsky et al. (2019) examined the superposed crater morphology as an indicator of target material characteristics; two cases were considered, where impact craters 80 to 160 m in diameter are superposed on RMDSs (Figures 10 and 11).

The 120-m crater superposed on a RMDS (Figure 10a) is characterized by a prominent but rounded rim, d/D = 0.09 and α ~12 deg. These data imply that it is of morphologic class BC (Basilevsky, 1976) (60-150 Ma), and the RMDS should be older. The presence of meter-sized rock boulders on the crater rim (Figure 10b) suggests a slightly younger age, approximately several tens of Ma (Basilevsky et al., 2015). The topographic profile of the crater (Figure 10c) appears regular and is unlike typical impacts into magmatic foam suggested by Wilson and Head (2017b). The presence of meter-sized boulders on the rim and inside the crater, and the prominently rounded rim crest both suggest its formation in a stratified target, with fragmental material overlying a more coherent rock target.

Figure 11 shows a second case, in which three craters are superposed on a 450-m diameter RMDS. Crater 1 is 170 m in diameter and craters 2 and 3 are each 80 m in diameter; Basilevsky et al. (2019) focused their analysis on craters 2 and 3.

The morphologic class (Figure 11a) of crater 1 is C (age ~300-600 Ma; Basilevsky et al., 2019). The 80-m craters 2 and 3 have prominent rims, d/D = 0.08 and 0.05 and α ~12 and 7 deg.; these are interpreted as craters of morphologic class BC transitional to C (crater 2) and class C (crater 3). The ages of these craters should be ~100-200 Ma (Basilevsky, 1976) or less than 500 Ma (Fassett & Thomson, 2014). The RMDS in Figure 11a should therefore be older than a few hundred Ma. Meter-sized boulders are clearly seen on the rim of crater 2 (Figure 11b), suggesting an age of the order of several tens of Ma (Basilevsky et al. 2015). Topographic profiles of the craters (Figure 11c) appear normal, in contrast to those predicted for impacts into magmatic foam (Head & Ivanov, 2019; Wilson & Head, 2017b). Baslievsky et al. (2019) interpreted the presence of these meter-sized boulders both on the rim and inside this crater to indicate that the superposed crater formation had occurred in a massive rock target, not in thick magmatic foam.

In summary, these examples of superposed craters suggest that the RMDS mound substrate is not composed of sufficiently large quantities of extremely vesicular magmatic foams to alter the impact energy partitioning and crater shape of superposing impact craters, casting doubt on simple models of a magmatic foam substrate.

6.2 The Lack of Inflationary Fracture Features Associated with RMDSs

One significant outstanding question regarding the hypothesis of an inflation origin of RMDSs (Wilson et al., 2019; Zhang et al., 2017, 2020) remains the absence of associated fracture features for RMDSs and their host mare unit, an important indicator for inflation mechanism in terrestrial basaltic flow fields. Lunar mare surfaces are mantled by a regolith layer of varying thickness up to ~10 meters (Bart et al., 2011, and references therein). The infilling and erasing of fracture/crack features by regolith development over billions of years are likely (Zhang et al., 2020).

The magmatic foam model (Wilson & Head, 2017b, 2018; Wilson et al., 2019) provides an alternative explanation for the absence of fractures associated with RMDSs and their host mare unit, and for the difficulty in discerning impact crater-like inflation pits (always with highly fractured margins in cases on Earth (Figures 8 and 9; e.g., Garry et al., 2012 and Hamilton et al., 2020). When a flow is emplaced, a more coherent and cooler boundary layer develops at the interface with both space and the cold substrate. As the flow continues to be fed at the source, the surface layer undergoes a process of expansion. The cooling magma will start releasing dissolved volatiles due to the crystallization process. Volatiles will concentrate in the residual magmatic liquid until it reaches saturation, and second boiling begins generating large quantities of small gas bubbles. The consequent volume expansion will cause an uplift of the brittle crust, thereby producing varying-size fractures on the flow surface. If these fractures extend into the lava containing the new gas bubbles, those bubbles are exposed to the vacuum and expand rapidly. The expansion process propagates back down onto the core of the flow expanding the original bubbles and creating new ones as the lava becomes exposed to lower pressure. This forces the foam that is being produced up into the cracks towards the surface of the crust, filling up the cracks as the foam infiltrates the older surface. Finally, the uppermost part of the foam layer reaches the hard vacuum causing the bubbles to burst, releasing gas, and generating a layer of glass fragments. This disintegration process extends down into the spreading foam and this produces a fine-grained fragmental layer with essentially no cohesive strength - a kind of instant regolith (autoregolith; see Head & Wilson, 2020) - at the top of the foam layer (Wilson & Head, 2017b; Wilson et al., 2019). It seems unlikely that this fragmental layer will have a surface appearance that reflects the cracks in the underlying original crust of the flow or even cracks in the foam itself as it cools. RMDSs formed in the Copernican period should have thinning regoliths and relatively undegraded morphologies. Thus, some of these types of formational structures could potentially be preserved, depending on the details of models proposed to account for their very young emplacement. Further examination of high-resolution images of RMDSs and their surroundings are required to assess these points as new hypotheses are developed for young RMDS formation.

6.3 Summary of Evidence for the "Young RMDS Emplacement Model"

Based on the characteristics outlined previously for the population of the RMDS (Zhang et al., 2017, 2020) and the stratigraphic and morphologic relationships documented in the specific preceding sections, we now summarize the implications for the general characteristics of the nature and mode of emplacement of RMDSs and use these to outline requirements for a new model for their emplacement: this differs significantly from the proposed mode of emplacement of RMDSs in connection with the host mare basalts, involving late-stage processes of flow inflation, cooling, second boiling, and extrusion of magmatic foams to the surface to produce the RMDSs (e.g., Wilson et al., 2019).

Stratigraphic superposition and embayment relationships displayed by several RMDSs and circular features on the host mare surface strongly suggest that the embaying RMDSs postdate the circular features. Although the formation of these craters by endogenic processes during lava flow emplacement cannot be confidently ruled out, the most likely origin for the embayed craters is superposed impact events, and this indicates that some unknown period of time elapsed between cooling of the host lava flow, formation of the embayed crater, and then embayment by the RMDS.

How much time elapsed between the superposed crater formation and the RMDS embayment? Analysis of the state of degradation of the craters and quantitative models of crater degradation indicate that the embayed craters are on the order of several hundred million years old (Figure 5 and Table 2). Although these are maximum ages (the RMDS could have formed and embayed the crater at any time after the formation age of the crater), they nonetheless indicate that the embaying RMDSs formed during the Copernican Period, several billion years later than the host lava flow. What are the absolute ages of these examples in the Copernican period? Unfortunately, these embaying RMDSs are too small to be dated reliably with superposed CSFD methods.

However, two other approaches support a young Copernican age not only for the RMDS-embayed crater examples, but for the whole RMDS population. Current models of diffusion-dominated landform degradation independently indicate that the dome-like structures and the morphologically and topographically distinct moats surrounding RMDSs could not have survived since the time of emplacement of the host lava flows. Secondly, regolith formation models indicate that continuous impact development of regolith in the time since emplacement of the host lava flows would have produced thicknesses up to, and in many cases exceeding, twice the amplitude of the topographic characteristics of RMDSs, and thus would have obliterated them if they had formed concurrently with the host lava flow regolith protolith.

Is there any further evidence to support the ancient origin of the RMDSs and their formation concurrently with the emplacement of their host lava flow? The Wilson et al. (2019) model predicts that the late-stage behavior of cooling lava flows favors extrusion of vesicle-rich foamy lavas onto the surface to produce the RMDS mounds, and concurrent subsidence of the lava flow surface to produce the surrounding moats. For some similar types mound of features associated with the Irregular Mare Patch Ina, Qiao et al. (2019) and Wilson and Head (2017b) have suggested that the mounds may be characterized by foamy lavas that have a highly vesicular and possibly aerogel-like structure: consequently, superposed impact craters might be characterized by a different morphology and morphometry. Basilevsky and Michael (2021), however, have presented evidence that impact craters superposed on the Ina floor mounds have morphologies that are comparable to those in the surrounding maria. Remaining uncertain from the model predictions, however, are the ranges of thicknesses of these foam layers, and the effects of the formation of an "autoregolith" by explosive modification of the upper layer of the extruded foams. Both factors need to be modeled to obtain a more specific picture of the original erupted and solidified substrate protolith (Head & Wilson, 2020) to test with observations of the morphology and morphometry of superposed impact craters formed subsequently.

In summary, these relationships strongly support a young Copernican-era age for the RMDS population, an age that postdates by more than two billion years that of its host lava flows, and thus appear to invalidate the ancient RMDS model of concurrent host-lava flow and RMDS formation (Wilson et al, 2019). However, quantitative measurements of 532 RMDSs in 12 different mare settings reveal some unique distribution patterns for their h/D ratios but within a constrained range 1/200 to 6/200 with the most common h/D ratio being around 4/200, which represents more than 30% of all RMDSs measured in each basin (Zhang et al., 2020; their Figure 5). The relative distribution of h/D illustrates that Procellarum and Fecunditatis show comparable overall distribution shapes peaking again at 0.02 (4/200) but with ratios skewed toward higher h/D values for Tranquillitatis. This means that there are subtle differences in RMDS morphology, and this would imply a wider time range for the formation of lunar RMDSs given that there is broad age diversity for the emplacement of RMDS-bearing mare flow units.

6.4 Outstanding Questions to Address in Formulating a Young RMDS Emplacement Model

Many uncertainties and outstanding questions remain concerning a Copernican age for RMDSs, including: 1) If the entire population of RMDSs is so young, why are RMDS-crater embayment relationships not much more common? It is more likely that there would be a wide time range for the formation of RMDSs considering that the RMDS-bearing mare units across the whole lunar surface have a broad age diversity (e.g., Hiesinger et al., 2011; Morota et al., 2011). 2) Why do the RMDSs have the same mineralogical affinities as their host lava flows, despite being erupted billions of years later? 3) The number of extrusive lunar basalt lava flow units peaks in the Imbrian and has significantly declined by the Eratosthenian, with no significant extrusive lava flows in the Copernican (e.g., Hiesinger et al., 2011). Despite this trend, RMDSs of apparent Copernican age are extremely widespread in the major lunar maria (Figure 1) (e.g., Zhang et al., 2020); 4) The occurrence of the youngest lunar lava flow units (Eratosthenian) is concentrated in the northern Oceanus Procellarum region (Hiesinger et al., 2011) and hypothesized to be related to the radioactive-element rich Procellarum KREEP Terrain crustal province (Jolliff et al., 2000). However, based on the RMDS distribution data (Figure 1) reported by Zhang et al. (2020), RMDSs occur in almost all other maria *except* the northern Oceanus Procellarum region; 5) If the RMDSs formed by Copernican-aged extrusive volcanism, what type of detailed model for the generation, ascent and eruption of magma is consistent with the emplacement of such small features and their associated moats, both individually, and in clusters, across virtually all the major maria of the Moon? 6) What global thermal evolution model(s) can account for such widespread Copernican-age volcanism? 7) Copernican-aged volcanism associated with the Irregular Mare Patches (IMPs) has been reported (Braden et al, 2014), but the ages and modes of emplacement have been debated (e.g., Qiao et al., 2017, 2019; Wilson & Head, 2017b). What are the similarities and differences between IMPs and RMDSs and how can this comparison better inform us about the nature of any Copernican-aged volcanism? These observations and characteristics then lead to a set of implications, constraints, requirements, and future research in association with models of Copernican-aged RMDS formation.

6.5 Some Requirements for a Young RMDS Emplacement Model

Based on our current understanding of the geological history of the Moon (summarized most recently in Jolliff et al., 2006), thermal structure in the Copernican is likely to be characterized by a very thick global lithosphere and a significantly compressional global state of stress in the lithosphere. Temperatures sufficiently high to induce partial melting and magma generation would occur only at great depths in the interior. Thus, during the Copernican, it would require significant volumes (a few hundred km^3) and very high overpressures (tens of MPa) to propagate magma-filled cracks (dikes) to the lunar surface (Wilson & Head, 2017a). The inevitable consequence of this is that when they reached the surface, such dikes would erupt large volumes of magma at initially high eruption rates (at least 10^5 m^3 s^{-1}) to form deposits matching the morphologies of large mare lava flows and sinuous rilles (Head & Wilson, 2017). These conditions are in stark contrast to the requirements for forming RMDSs: small (10^4-10^5 m^3) volumes of magma erupted at low effusion rates (Zhang et al., 2020). Furthermore, since RMDSs generally have similar compositions to those of the mare lavas on which they are emplaced, their magma source regions would be required to have mineralogies that are the same as those characterizing the surface lavas that erupted several billion years before RMDS emplacement. Upon erupting at the surface, the lavas must be able to form one or more very small-volume, convex-upward mounds (more viscous magma?), surrounded by a moat, and not to form any associated volcanic landforms (lava flows, cones, small shields, pyroclastics, linear vents, associated graben, etc.).

Garrick-Bethell and Seritan (2021) have suggested that geologically recent laccolithic intrusions beneath appropriately sized impact craters in ancient lava flows could induce RMDS-like topography on the surface, but this model does not explain all RMDS features, especially the relatively wide moats. This explanation also suffers from the same problem as any small-volume, recent activity: the need to fine-tune the volume of magma getting close to the surface (Zhang et al., 2020). In summary, no model able to explain how recent volcanism could emplace features with the size range characterizing RMDSs exists. While further work on magma transport to the surface might help to shed light on this problem, a fundamental examination of the assumptions and interpretations that are the basis for our current understanding of the geological and thermal evolution of the Moon’s deep interior (e.g., Jolliff et al., 2006) may also be warranted.

6.6 Future Research and Exploration Designed to Address and Resolve the RMDS Age of Emplacement Conundrum

The genesis and evolution of the RMDSs could represent the target of future lunar exploration missions guided by the testable hypotheses formulated in this work. Both robotic and human exploration missions could help unravel their age and mode of formation. Robotic exploration with stationary landers on individual RMDSs could determine the nature of the regolith and assess the presence of highly vesicular basalts and magmatic foams predicted by the “contemporaneous” model. Absolute ages could also be estimated, even allowing for low precision and a relatively large uncertainty window of hundreds of millions of years: this would suffice to resolve the Imbrian versus Copernican age predictions of the two hypotheses.

Robotic rovers could traverse the domes, the moats, and the surrounding mare terrains, searching for definitive evidence of age differences and feature (mound, moat) origins. Ground-penetrating radar, as recently employed on Chang’e 3 and 4 missions (e.g., Lai et al., 2019), would significantly help to resolve these issues (for example, detection of a post-host-unit, pre-RMDS regolith substrate layer representing accumulation during the several billion years interval predicted to occur in the Copernican-RMDS model). Robotic samples return (such as recently accomplished by Chang’e 5) from a RMDS mound summit would address most outstanding questions.

Of course, the ideal exploration scenario would include human exploration, as accomplished during the Apollo Lunar Exploration Program, which would add an informed and flexible survey of stratigraphic relationships and take advantage of serendipitous opportunities. Thus, the quest for the origin and age of the RMDSs represents an important potential target for all levels of future lunar exploration.

7. Conclusions

Ring-Moat Dome Structures (RMDSs) have recently been documented in most of the major lunar maria: they are small circular mounds (average diameter ~200 m) ~3-4 m in height, surrounded by narrow, shallow moats, occurring in clusters, and are widespread in ancient Imbrian-aged mare basalt host units, showing mineralogies similar to their host units. A formation model to explain the co-occurrence and related genesis of RMDSs and their host flow unit has been proposed (Wilson et al., 2019). In this emplacement model, lava flow inflation and second boiling result in significant degassing of volatiles to produce magmatic foams, and cause crustal cracking and extrusion of foams to produce domes and their related ring moats. This model concludes that RMDS occurrences represent late-stage inflation and degassing activity in the waning stages of flow emplacement, cooling, and solidification. Thus, RMDSs are coincident in time with the emplacement of the flow, consistent with the similar mineralogy of the flow and the RMDSs.

Several lines of evidence suggest, however, that the RMDS did not form contemporaneously with the host flow emplacement, but rather formed in the Copernican Period (~1.1 Ga to present), 1-3 billion years after the emplacement and solidification of the host lava flows. Several cases of embayment of RMDS domes into circular depressions (and thus their superposition and younger age) are reported. Based on the high likelihood that these circular depressions are of impact origin, the degradation states of the underlying embayed craters can be used to estimate the maximum age of embayment, resulting in estimate Copernican ages (~1.1 Ga – present) of mound emplacement and embayment. Additional supporting evidence for a much younger age independent of the host mare basalt unit comes from crater degradation age and regolith thickness models. The ages of the RMDS host lava flows are typically in the range of 2-3.7 Ga. Regolith development models on lunar basaltic lava flows predict that the thickness of regolith on top of lava flows of these ages should be in the 5-10 m range, comparable to the vertical relief of domes and significantly exceeding the vertical relief of the moats. The observations favor a much younger RMDS emplacement age. The synchronous emplacement model also predicts unusual surface properties for the RMDS substrate. However, initial examination of craters superposed on RMDSs suggests that their morphologies are comparable to those occurring in normal maria.

To address this fundamental age contradiction for RMDS emplacement, we outlined the detailed nature of these contradictions, described candidate requirements for a young RMDS emplacement model, and concluded with a discussion of key exploration goals and objectives that could help clarify and resolve this very significant conundrum for the geological and thermal evolution of the Moon.

Data Availability Statement

The imagery of LROC NACs used in this work is archived in the Geophysics Nodes of the Planetary Data System (PDS). All the over 8000 RMDSs presented in Figure 1 can be found at the Zenodo.org. (Zhang, F. et al., 2020a, Zenodo, http://doi.org/10.5281/zenodo.3711659). The NAC-based DEMs used for estimating the ages of RMDS-overlapped craters (Figs. 2a-2c, corresponding to areas A2, A4, and A7) with a locally calibrated Monte Carlo model are also available online (Zhang, F. et al., 2020b, Zenodo, http://doi.org/10.5281/zenodo.3748825).

Acknowledgements

This research was supported by the Science and Technology Development Fund, Macau SAR (File No. 0049/2020/A1), the National Natural Science Foundation of China (Grants No. 11903090 and 11941001), and the National Key R&D Program of China (Grant No. 2020YFE0202100). The authors would like to thank K. Fisher for providing the crater annotation data used for CNN training. TW and CW were funded by the Deutsche Forschungsgemeinschaft (DFG, German Research Foundation), Project number 269661170. The authors would like to thank the Editor Bradley Thomson and two anonymous reviewers for their constructive comments and suggestions.

References

Anthony, E. Y., & Poths, J. (1992). 3He surface exposure dating and its implications for magma evolution in the Potrillo volcanic field, Rio Grande Rift, New Mexico, USA. *Geochimica et Cosmochimica Acta*, *56*(11), 4105-4108. https://doi.org/10.1016/0016-7037(92)90022-B

Bart, G. D., Nickerson, R. D., Lawder, M. T., & Melosh, H. J. (2011). Global survey of lunar regolith depths from LROC images. *Icarus*, *215*(2), 485-490. https://doi.org/10.1016/j.icarus.2011.07.017

Basilevsky, A. T. (1974). Estimation of thickness and degree of reworking of lunar regolith from the crater spatial densities. *Kosmicheskie Issledovaniya*. V. XII. Issue 4. 606-609. (In Russian).

Basilevsky, A. T. (1976). On the evolution rate of small lunar craters. In *7th Lunar and Planetary Science Conference*, The Woodlands, TX, 1,005-1,020.

Basilevsky, A. T., 2015. Estimation of absolute age of impact craters of the Moon, Mercury and Mars based on the degree of their morphologic prominence. In *Study of the Solar system: The space milestones. Proceedings of the Scientific Session devoted to 80th jubilee of Academician M. Ya. Marov*. Space Research Institute. Moscow. 213-228.

Basilevsky, A. T., Florensky, C. P., & Ronca, L. B. (1977). A possible lunar outcrop: A study of Lunokhod-2 data. *The moon*, *17*(1), 19-28. https://doi.org/10.1007/BF00566850

Basilevsky, A. T., & Michael, G. G. (2021). Lunar Crater Ina: Analysis of the Morphology of Intercrater Landforms. *Solar System Research*, *55*(1)**,** 20–30. https://doi.org/10.1134/S0038094621010020

Basilevsky, A. T., Zhang, F., Wöhler, C., Bugiolacchi, R., Head, J. W., & Wilson, L. (2019). Lunar Ring-Moat Dome Structures and Their Relationships with Small Impact Craters. In *50th Lunar and Planetary Science Conference*, The Woodlands, TX (abstract #1507).

Bennett, K. A., Horgan, B. H. N., Bell, J. F., Meyer, H. M., & Robinson, M. S. (2015). Moon Mineralogy Mapper investigation of the Ina irregular mare patch. In *46th Lunar and Planetary Science Conference*, The Woodlands, TX (abstract #2646).

Borg, L. E., Shearer, C. K., Asmerom, Y., & Papike, J. J. (2004). Prolonged

KREEP magmatism on the Moon indicated by the youngest dated lunar igneous rock. *Nature*, *432*(7014), 209-211. https://doi.org/10.1038/nature03070

Borg, L. E., Gaffney, A. M., & Shearer, C. K. (2015). A review of lunar chronology revealing a preponderance of 4.34–4.37 Ga ages. *Meteoritics & Planetary Science*, *50*(4), 715-732. https://doi.org/10.1111/maps.12373

Braden, S. E., Stopar, J. D., Robinson, M. S., Lawrence, S. J., Van Der Bogert, C. H., & Hiesinger, H. (2014). Evidence for basaltic volcanism on the Moon within the past 100 million years. *Nature Geoscience*, *7*(11), 787-791. https://doi.org/10.1038/ngeo2252

Bugiolacchi, R., & Wöhler, C. (2020), Small craters population as a useful geological investigative tool: Apollo 17 region as a case study, *Icarus*, *350*, 113927. https://doi.org/10.1016/j.icarus.2020.113927

De Hon, R. A., & Earl, R. A. (2018). Reassessment of features in the Aden Crater lava flows, Dona Ana County, New Mexico. *New Mexico Geology*, *40*(1), 17-26.

Fassett, C. I., Minton, D. A., Thomson, B. J., Hirabayashi, M., & Watters, W. A. (2018). Re-analysis of observations of crater degradation on the lunar maria accounting for anomalous diffusion. In *49th Lunar and Planetary Science Conference*, The Woodlands, TX (abstract #1502).

Fassett, C. I., & Thomson, B. J. (2014). Crater degradation on the lunar maria: Topographic diffusion and the rate of erosion on the Moon. *Journal of Geophysical Research: Planets*, *119*(10), 2255-2271. https://doi.org/10.1002/2014JE004698

Fernandes, V. A., Burgess, R., Bischoff, A., Sokol, A. K., & Haloda, J. (2007). Kalahari 009 and North East Africa 003: Young (< 2.5 Ga) lunar mare basalts. In *38th Lunar and Planetary Science Conference*, The Woodlands, TX (abstract #1611).

Fisher, K. (2014). An age for Hell Q from small diameter craters. In *45th Lunar and Planetary Science Conference*, The Woodlands, TX (abstract #1421).

Garrick-Bethell, I., & Seritan, M. R. (2021). Laccolith model for lunar Ring-moat Dome Structures. In *52th Lunar and Planetary Science Conference*, The Woodlands, TX (abstract 2369).

Garry, W. B., Robinson, M. S., Zimbelman, J. R., Bleacher, J. E., Hawke, B. R., Crumpler, L. S., et al. (2012). The origin of Ina: Evidence for inflated lava flows on the Moon. *Journal of Geophysical Research: Planets*, 117(E12), E00H31. https://doi.org/10.1029/2011JE003981

Gelman, A., Carlin, J. B., Stern, H. S., Dunson, D. B., Vehtari, A., & Rubin, D. B. (2013). *Bayesian data analysis*. CRC press.

Greeley, R. (1970). Terrestrial analogs to lunar dimple (drainage) craters. *The moon*, *1*(2), 237-252. https://doi.org/10.1007/BF00562828

Greeley, R., & Gault, D. E. (1971). Endogenetic craters interpreted from crater counts on the inner wall of Copernicus. *Science*, *171*(3970), 477-479. DOI: 10.1126/science.171.3970.477

Greeley, R., & Gault, D. E. (1979). Endogenic craters on basaltic lava flows-Size frequency distributions. In *10th Lunar and Planetary Science Conference Proceedings*, The Woodlands, TX, 2,919-2,933.

Grimes, K. G. (2008). Small Subcrustal Lava Caves: Examples from Victoria, Australia. In *Proceedings of the X, XI, and XII International symposia on Vulcanospeleology*, Association for Mexican Cave Studies Bulletin (Vol. 19, pp. 35-44).

Grumpe, A., & Wöhler, C. (2014). Recovery of elevation from estimated gradient fields constrained by digital elevation maps of lower lateral resolution. *ISPRS Journal of Photogrammetry and Remote Sensing*, *94*, 37-54. https://doi.org/10.1016/j.isprsjprs.2014.04.011

Grumpe, A., Schröer, C., Kauffmann, S., Fricke, T., Wöhler, C., & Mall, U. (2016). Refinement of stereo image analysis using photometric shape recovery as an alternative to bundle adjustment. *International Archives of the Photogrammetry*, Remote Sensing & Spatial Information Sciences, vol. XLI-B4, p. 565-572.

Hamilton, C. W., Scheidt, S. P., Sori, M. M., de Wet, A. P., Bleacher, J. E., Mouginis-Mark, P. J., et al. (2020). Lava-Rise Plateaus and Inflation Pits in the McCartys Lava Flow Field, New Mexico: An Analog for Pāhoehoe-Like Lava Flows on Planetary Surfaces. *Journal of Geophysical Research: Planets*, *125*(7), e2019JE005975. https://doi.org/10.1029/2019JE005975

Hartmann, W. K., Quantin, C., & Mangold, N. (2007). Possible long-term decline in impact rates: 2. Lunar impact-melt data regarding impact history. *Icarus*, *186*(1), 11-23. https://doi.org/10.1016/j.icarus.2006.09.009

Head, J. W. (1976). Lunar volcanism in space and time. *Reviews of Geophysics*, *14*(2), 265-300. https://doi.org/10.1029/RG014i002p00265

Head, J. W., & Ivanov, B. A. (2019). Ina irregular mare patch (IMP): New insights from observations of superposed impact craters. *The 10th Moscow Solar System Symposium*, Space Research Institute, Moscow, Russia, abstract #MS3-PS-32.

Head, J. W., & Wilson, L. (2017). Generation, ascent and eruption of magma on the Moon: New insights into source depths, magma supply, intrusions and effusive/explosive eruptions (Part 2: Predicted emplacement processes and observations). *Icarus*, *283*, 176-223. https://doi.org/10.1016/j.icarus.2016.05.031

Head, J. W., & Wilson, L. (2020). Rethinking lunar mare basalt regolith formation: new concepts of lava flow protolith and evolution of regolith thickness and internal structure. *Geophysical Research Letters*, *47*(20), e2020GL088334. https://doi.org/10.1029/2020GL088334

Hess, P. C., & Parmentier, E. M. (1995). A model for the thermal and chemical evolution of the Moon's interior: Implications for the onset of mare volcanism. *Earth and Planetary Science Letters*, *134*(3-4), 501-514. https://doi.org/10.1016/0012-821X(95)00138-3

Hiesinger, H., Head, J. W., Wolf, U., Jaumann, R., & Neukum, G. (2006). New ages for basalts in Mare Fecunditatis based on crater size-frequency measurements. In *37th Lunar and Planetary Science Conference*, The Woodlands, TX (abstract #1151).

Hiesinger, H., Head, J. W., Wolf, U., Jaumann, R., & Neukum, G. (2011). Ages and stratigraphy of lunar mare basalts: A synthesis. *Recent Advances and Current Research Issues in Lunar Stratigraphy: Geological Society of America Special Paper*, *477*, 1-51. DOI: 10.1130/2011.2477(01)

Hoffer, J. M. (1976). Geology of the Potrillo basalt field, south-central New Mexico. *New Mexico Bureau of Mines and Mineral Resources*, Circular *149*, 1-30.

Hon, K. E. N., Kauahikaua, J. I. M., Denlinger, R., & Mackay, K. (1994). Emplacement and inflation of pahoehoe sheet flows: Observations and measurements of active lava flows on Kilauea Volcano, Hawaii. *Geological Society of America Bulletin*, *106*(3), 351-370. https://doi.org/10.1130/0016-7606(1994)106<0351:EAIOPS>2.3.CO;2

Jolliff, B. L., Gillis, J. J., Haskin, L. A., Korotev, R. L., & Wieczorek, M. A. (2000). Major lunar crustal terranes: Surface expressions and crust-mantle origins. *Journal of Geophysical Research: Planets*, *105*(E2), 4197-4216. https://doi.org/10.1029/1999JE001103

Joliff, B., Wieczorek, M., Shearer, C., Neal, C. (Eds.). (2006). New views of the Moon. *Vol. 60 of Reviews in mineralogy & geochemistry*. Mineralogical Society of America and the Geochemical Society.

Kreslavsky, M. A., Head, J. W., Neumann, G. A., Zuber, M. T., & Smith, D. E. (2017). Low-amplitude topographic features and textures on the Moon: Initial results from detrended Lunar Orbiter Laser Altimeter (LOLA) topography. *Icarus*, *283*, 138-145. https://doi.org/10.1016/j.icarus.2016.07.017

Lai, J., Xu, Y., Zhang, X., Xiao, L., Yan, Q., Meng, X., et al. (2019). Comparison of Dielectric Properties and Structure of Lunar Regolith at Chang'e-3 and Chang'e-4 Landing Sites Revealed by Ground-Penetrating Radar. *Geophysical Research Letters*, *46*(22), 12,783-12,793. https://doi.org/10.1029/2019GL084458

McEwen, A. S., & Bierhaus, E. B. (2006). The importance of secondary cratering to age constraints on planetary surfaces. *Annual Review of Earth and Planetary Science*, *34*, 535-567. https://doi.org/10.1146/annurev.earth.34.031405.125018

McKay, D. S., Heiken G., Basu A, Blanford G., Simon S., Reedy R., French B. M., & Papike J. (1991). The lunar regolith. In: *Lunar Source Book: A User Guide to the Moon*. G.H. Heiken, D.T. Vaniman, B.M. French eds., Cambridge University Press, 285-356.

Morota, T., Haruyama, J., Ohtake, M., Matsunaga, T., Honda, C., Yokota, Y., et al. (2011). Timing and characteristics of the latest mare eruption on the Moon. *Earth and Planetary Science Letters*, *302*(3-4), 255-266. https://doi.org/10.1016/j.epsl.2010.12.028

Neukum, G., Ivanov, B., & Hartmann, W. (2001). Cratering records in the inner solar system in relation to the lunar reference system. *Space Science Reviews*, *96*, 55–86. https:// doi.org/10.1023/A:1011989004263.

Ollier, C. D. (1964). Tumuli and lava blisters of Victoria, Australia. *Nature*, *202*(4939), 1284-1286. https://doi.org/10.1038/2021284a0

Qiao, L., Head, J., Wilson, L., Xiao, L., Kreslavsky, M., & Dufek, J. (2017). Ina pit crater on the Moon: Extrusion of waning-stage lava lake magmatic foam results in extremely young crater retention ages. *Geology*, *45*(5), 455-458. https://doi.org/10.1130/G38594.1

Qiao, L., Head, J. W., Ling, Z., Wilson, L., Xiao, L., Dufek, J. D., & Yan, J. (2019). Geological characterization of the Ina shield volcano summit pit crater on the Moon: Evidence for extrusion of waning-stage lava lake magmatic foams and anomalously young crater retention ages. *Journal of Geophysical Research: Planets*, *124*(4), 1100-1140. https://doi.org/10.1029/2018JE005841

Robinson, M. S., Brylow, S. M., Tschimmel, M., Humm, D., Lawrence, S. J., Thomas, P. C., et al. (2010). Lunar reconnaissance orbiter camera (LROC) instrument overview. *Space Science Reviews*, *150*(1-4), 81-124. https://doi.org/10.1007/s11214-010-9634-2

Schultz, P. H., & Greeley, R. (1976). Ring-moat structures: Preserved flow morphology on lunar maria. In *7th Lunar and Planetary Science Conference*, The Woodlands, TX, 788–789.

Schultz, P. H., Greeley, R., & Gault, D. (1976). Degradation of small mare surface features. In *7th Lunar and Planetary Science Conference*, The Woodlands, TX, 985–1003.

Schultz, P. H., & Spudis, P. D. (1983). Beginning and end of lunar mare volcanism. *Nature*, *302*(5905), 233-236. https://doi.org/10.1038/302233a0

Schultz, P. H., Staid, M. I., & Pieters, C. M. (2006). Lunar activity from recent gas release. *Nature*, *444*(7116), 184-186. https://doi.org/10.1038/nature05303

Self, S., Keszthelyi, L., & Thordarson, T. (1998). The importance of pāhoehoe. *Annual Review of Earth and Planetary Sciences*, *26*(1), 81-110. https://doi.org/10.1146/annurev.earth.26.1.81

Shearer, C. K., Hess, P. C., Wieczorek, M. A., Pritchard, M. E., Parmentier, E. M., Borg, L. E., et al. (2006). Thermal and magmatic evolution of the Moon. *Reviews in Mineralogy and Geochemistry*, *60*(1), 365-518. https://doi.org/10.2138/rmg.2006.60.4

Shkuratov, Y. G., & Bondarenko, N. V. (2001). Regolith layer thickness mapping of the Moon by radar and optical data. *Icarus*, *149*(2), 329-338. https://doi.org/10.1006/icar.2000.6545

Shoemaker, E. M., Batson, R. M., Holt, H. E., Morris, E. C., Rennilson, J. J., & Whitaker, E. A. (1969). Observations of the lunar regolith and the Earth from the television camera on Surveyor 7. *Journal of Geophysical Research*, *74*(25), 6081-6119. https://doi.org/10.1029/JB074i025p06081

Sinha, R. K., Sivaprahasam, V., Bhatt, M., Kumari, N., Srivastava, N., Varatharajan, I., et al. (2020). Geological characterization of Chandrayaan-2 landing site in the southern high latitudes of the Moon. *Icarus*, *337*, 113449. https://doi.org/10.1016/j.icarus.2019.113449

Snoek, J., Larochelle, H., & Adams, R. P. (2012). Practical Bayesian Optimization of Machine Learning Algorithms. *Preprint*, arXiv:1206.2944. https://arxiv.org/abs/1206.2944v2

Solomon, S. C. (1978). On volcanism and thermal tectonics on one-plate planets. *Geophysical Research Letters*, *5*(6), 461-464. https://doi.org/10.1029/GL005i006p00461

Solomon, S. C. (1986). On the early thermal state of the Moon. In Hartmann, W. K., et al., eds., Origin of the Moon, Houston, Texas, Lunar and Planetary Institute, 435-452.

Spohn, T., Konrad, W., Breuer, D., & Ziethe, R. (2001). The longevity of lunar volcanism: Implications of thermal evolution calculations with 2D and 3D mantle convection models. *Icarus*, *149*, 54-65. https://doi.org/10.1006/icar.2000.6514

Stöffler, D., Ryder, G., Ivanov, B. A., Artemieva, N. A., Cintala, M. J., & Grieve, R. A. (2006). Cratering history and lunar chronology. *Reviews in Mineralogy and Geochemistry*, *60*(1), 519-596. https://doi.org/10.2138/rmg.2006.60.05

Swann G. A., Bailey N. G., Batson R. M., Freeman, V. L., Hait, M. H., Head, J. W., et al. (1972). Preliminary Geologic Investigation of the Apollo 15 Landing Site. In: *APOLLO 15 PRELIMINARY SCIENCE REPORT*. NASA. Washington, D.C. 5-1 – 5-112.

Taylor, L. A., Shervais, J. W., Hunter, R. H., Shih, C. Y., Bansal, B. M., Wooden, J., et al. (1983). Pre-4.2 AE mare-basalt volcanism in the lunar highlands. *Earth and Planetary Science Letters*, *66*, 33-47. https://doi.org/10.1016/0012-821X(83)90124-3

Terada, K., Anand, M., Sokol, A. K., Bischoff, A., & Sano, Y. (2007). Cryptomare magmatism 4.35 Gyr ago recorded in lunar meteorite Kalahari 009. *Nature*, *450*(7171), 849-852. https://doi.org/10.1038/nature06356

Van der Bogert, C. H., Michael, G., Kneissl, T., Hiesinger, H., & Pasckert, J. H. (2015). Development of guidelines for recommended lunar CSFD count area sizes via analysis of random CSFDs. *Workshop on Issues in Crater Studies and the Dating of Planetary Surfaces*, abstract #9023.

Wagner, R. V., Speyerer, E. J., Robinson, M. S., & Team, L.R.O.C., 2015. New mosaicked data products from the LROC team. In *46th Lunar and Planetary Science Conference*. The Woodlands, TX (abstract 1473).

Walker, G. P. 1991. Structure, and origin by injection of lava under surface crust, of tumuli,“lava rises”,“lava-rise pits”, and “lava-inflation clefts” in Hawaii. *Bulletin of Volcanology*, *53*(7), 546-558. https://doi.org/10.1007/BF00298155

Wieczorek, M. A., Jolliff, B. L., Khan, A., Pritchard, M. E., Weiss, B. P., Williams, J. G., et al. (2006). The constitution and structure of the lunar interior. *Reviews in Mineralogy and Geochemistry*, *60*(1), 221-364. https://doi.org/10.2138/rmg.2006.60.3

Wilhelm, T., & Wöhler, C. (2021). Uncertainty Guided Recognition of Tiny Craters on the Moon. *Proc. Int. Conf. on Pattern Recognition*, pp. 5198-5205, Milano, Italy (online).

Williams, D. A., Fagents, S. A., & Greeley, R. (2000). A reassessment of the emplacement and erosional potential of turbulent, low-viscosity lavas on the Moon. *Journal of Geophysical Research: Planets*, *105*(E8), 20189-20205. https://doi.org/10.1029/1999JE001220

Williams, J. P., van der Bogert, C. H., Pathare, A. V., Michael, G. G., Kirchoff, M. R., & Hiesinger, H. (2018). Dating very young planetary surfaces from crater statistics: A review of issues and challenges. *Meteoritics & Planetary Science*, *53*(4), 554-582. https://doi.org/10.1111/maps.12924

Wilson, L., & Head, J. W. (2017a). Generation, ascent and eruption of magma on the Moon: New insights into source depths, magma supply, intrusions and effusive/explosive eruptions (Part 1: Theory). *Icarus*, *283*, 146-175. https://doi.org/10.1016/j.icarus.2015.12.039

Wilson, L., & Head, J. W. (2017b). Eruption of magmatic foams on the Moon: Formation in the waning stages of dike emplacement events as an explanation of “irregular mare patches”. *Journal of Volcanology and Geothermal Research*, *335*, 113-127. https://doi.org/10.1016/j.jvolgeores.2017.02.009

Wilson, L., & Head, J. W. (2018). Controls on lunar basaltic volcanic eruption structure and morphology: Gas release patterns in sequential eruption phases. *Geophysical Research Letters*, *45*(12), 5852-5859. https://doi.org/10.1029/2018GL078327

Wilson, L., Head, J. W., & Zhang, F. (2019). A theoretical model for the formation of Ring Moat Dome Structures: Products of second boiling in lunar basaltic lava flows. *Journal of Volcanology and Geothermal Research*, *374*, 160-180. https://doi.org/10.1016/j.jvolgeores.2019.02.018

Xiao, Z., & Werner, S. C. (2015). Size-frequency distribution of crater populations in equilibrium on the Moon. *Journal of Geophysical Research: Planets*, *120*(12), 2277-2292. https://doi.org/10.1002/2015JE004860

Xie, M., Zhu, M. H., Xiao, Z., Wu, Y., & Xu, A. (2017). Effect of topography degradation on crater size-frequency distributions: Implications for populations of small craters and age dating. *Geophysical Research Letters*, *44*(20), 10,171-10,179. https://doi.org/10.1002/2017GL075298

Zhang, F., Head, J. W., Basilevsky, A. T., Bugiolacchi, R., Komatsu, G., Wilson, L., et al. (2017). Newly discovered ring-moat dome structures in the lunar maria: Possible origins and implications. *Geophysical Research Letters*, *44*(18), 9216-9224. https://doi.org/10.1002/2017GL074416

Zhang, F., Wöhler, C., Head, J. W., Bugiolacchi, R., Wilson, L., & Grumpe, A. (2018). Ring-Moat Dome Structures (RMDSs) in the Lunar Maria: Further Statistical and Morphological Characterization. In *49th Lunar and Planetary Science Conference*, The Woodlands, TX (abstract #1374).

Zhang, F., Head, J. W., Wöhler, C., Bugiolacchi, R., Wilson, L., Basilevsky, A. T., et al. (2020). Ring-Moat Dome Structures (RMDSs) in the lunar maria: Statistical, compositional, and morphological characterization and assessment of theories of origin. *Journal of Geophysical Research: Planets*, *125*(7), e2019JE005967. https://doi.org/10.1029/2019JE005967

Zhang, F., Head, J. W., Wöhler, C., Bugiolacchi, R., Wilson, L., Basilevsky, A. T., et al. (2020a). Locations and derived diameters of RMDSs as per Fig. 6 and all the

8281 RMDSs identified so far across the global Moon by March, 2020 [Data set]. Zenodo. http://doi.org/10.5281/zenodo.3711659

Zhang, F., Head, J. W., Wöhler, C., Bugiolacchi, R., Wilson, L., Basilevsky, A. T., et al. (2020b). LROC NAC-based high-resolution (2 m per pixel) digital elevation models (DEMs) of twelve regions on the Moon containing ring-moat dome structures (RMDSs) [Data set]. Zenodo. http://doi.org/10.5281/zenodo.3748825

Ziethe, R., Seiferlin, K., & Hiesinger, H. (2009). Duration and extent of lunar volcanism: Comparison of 3D convection models to mare basalt ages. *Planetary and Space Science*, *57*(7), 784-796. https://doi.org/10.1016/j.pss.2009.02.002

Figures Captions:

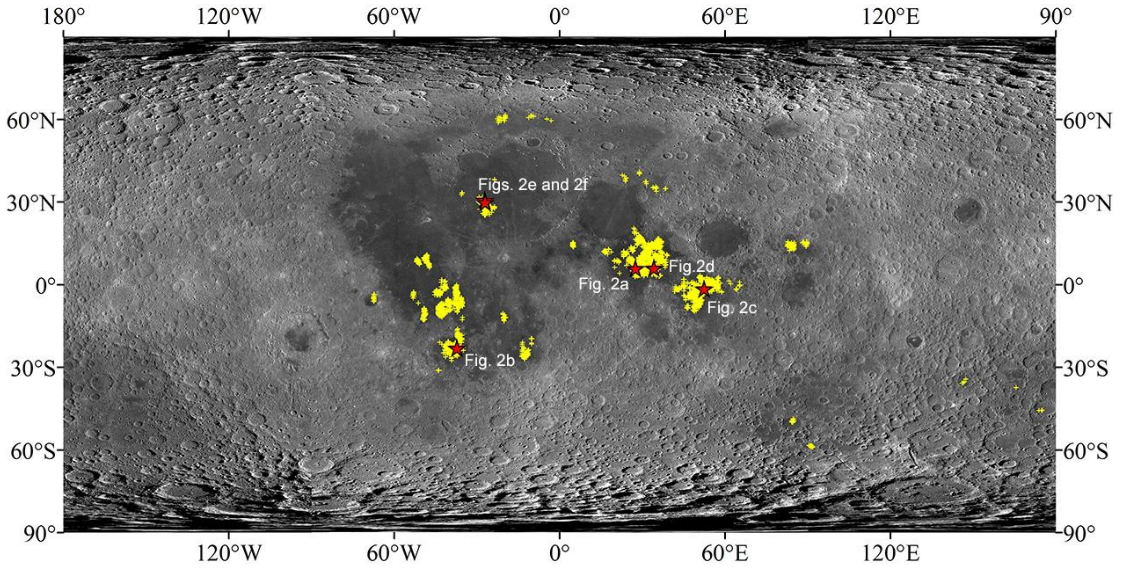

Figure 1. The global distribution of more than 8,000 RMDSs (yellow crosses) on the Moon (Zhang et al., 2020). The red stars indicate the locations of the RMDS-superposed craters analyzed in this study, as shown in Figure 2. The base map is the LROC WAC Global Morphology Mosaic 100 m (at 643 nm; Wagner et al., 2015).

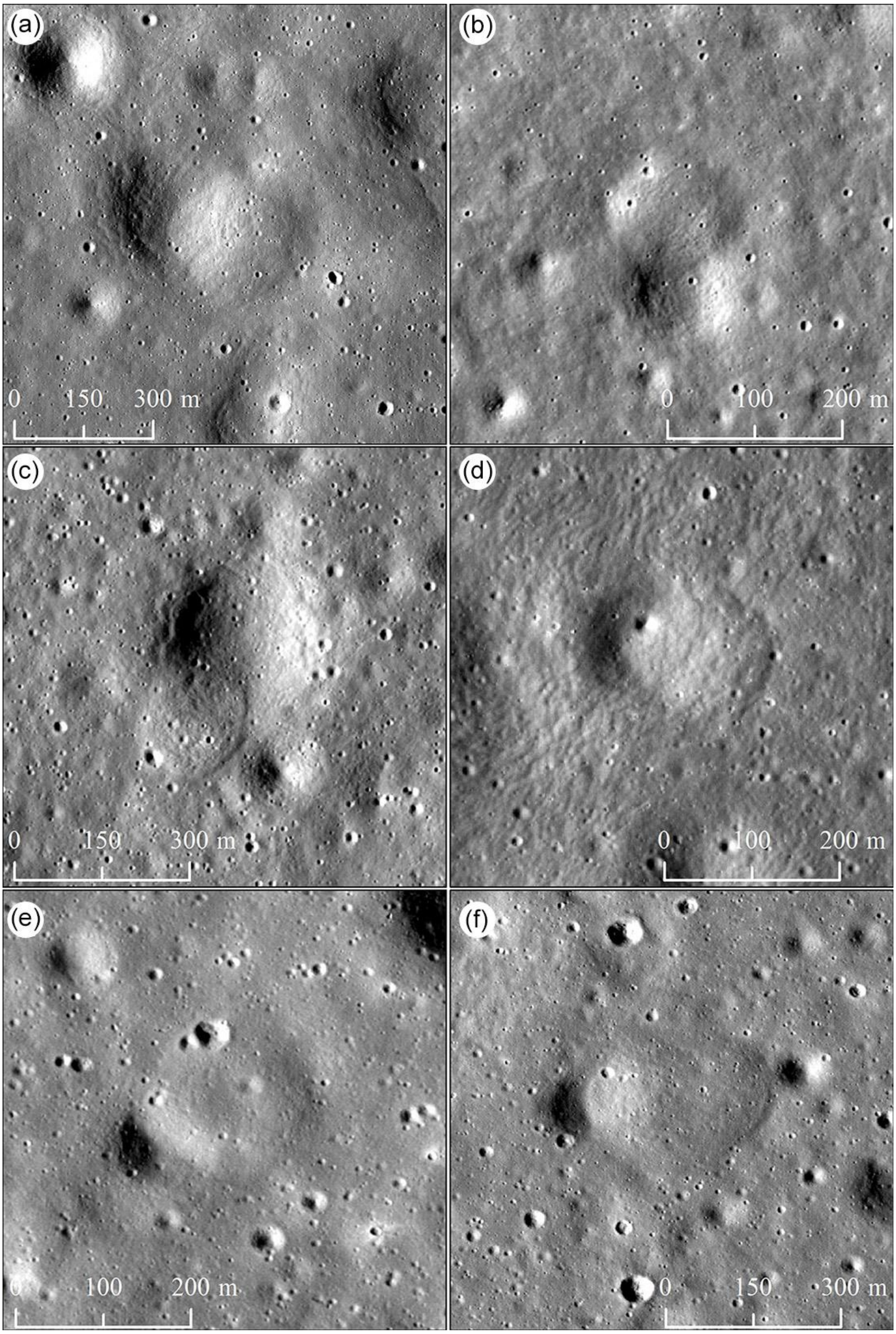

Figure 2. LROC NAC images for confirmed RMDS-superposed craters analyzed in this study. Their location coordinates, hosting mare, and NAC frame used are: (a) (5.935°N, 27.456°E), Tranquillitatis, M1172873803LE; (b) (22.967°S, 37.294°W), Humorum, M1142680981LE; (c) (1.461°S, 52.39°E), Fecunditatis, M1126787189LE;

(d) (6.028°N, 34.19°E), Tranquillitatis, M180944663RE; (e) (30.704°N, 27.222°W), Imbrium, M181352550RE; (f) (29.885°N, 27.077°W), Imbrium, M181352550RE.

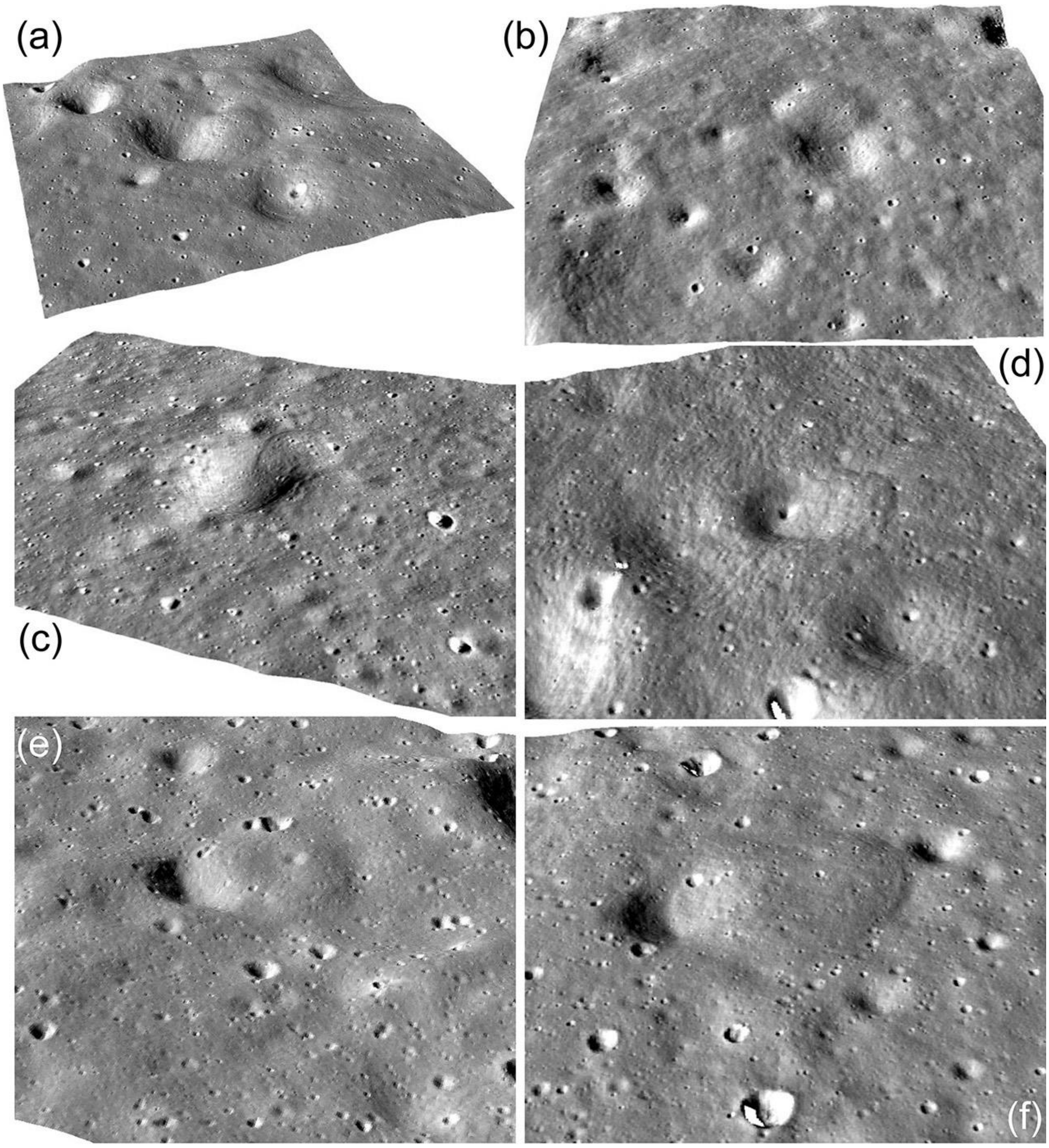

Figure 3. Three-dimensional views of RMDSs embayment into adjacent craters, corresponding to the individual cases illustrated in Figure 2. The 3D views are created based on NACs draping over NAC-based DEMs (2 m/pixel, 6× vertical exaggeration).

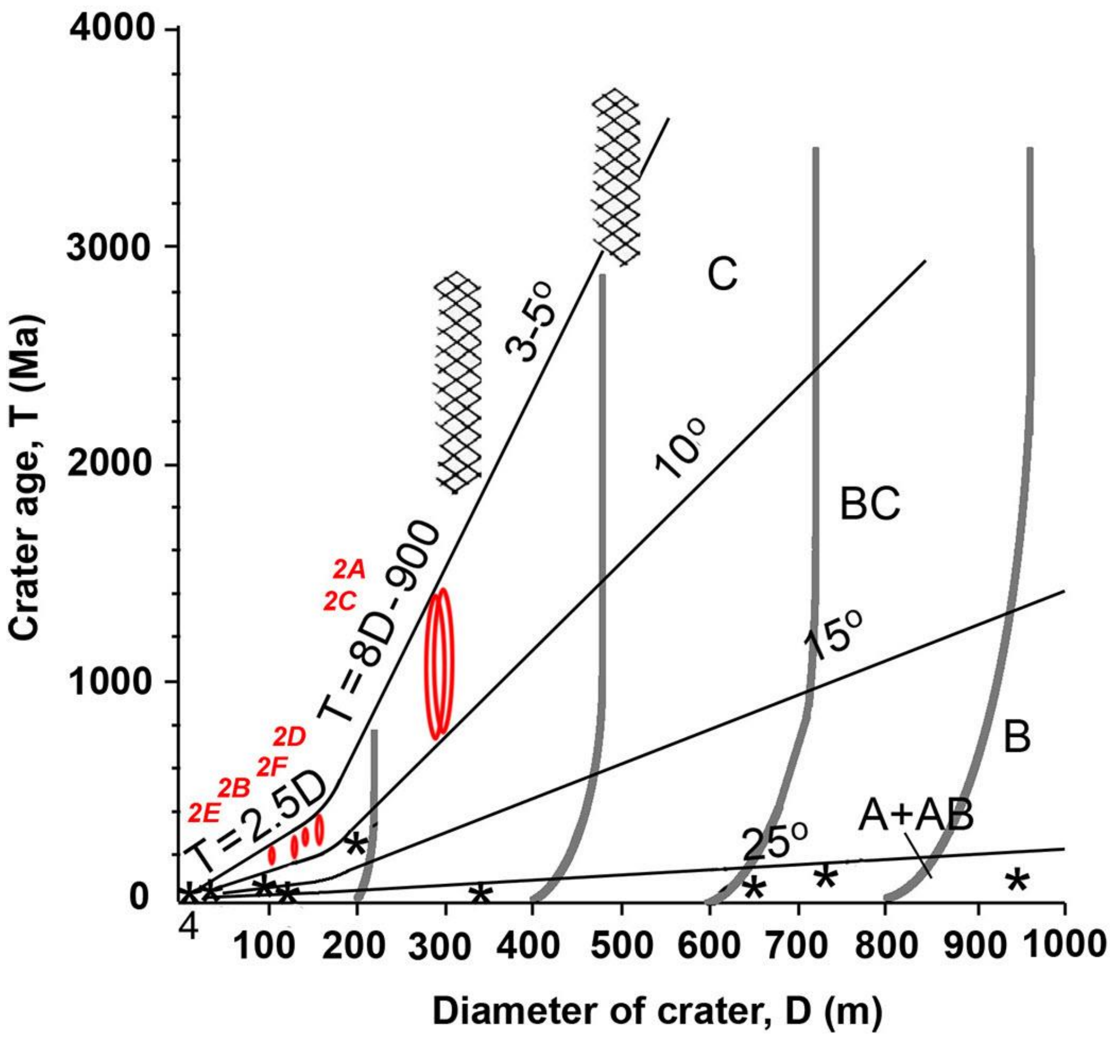

Figure 4. Ages of craters superposed by RMDS (red) on the diagram of the dependence of absolute age of craters on their diameters and the degree of their morphologic maturity - classes A, AB, B, BC and C. The typical values of maximum steepness of inner slopes of craters of different classes are shown along with the boundary lines. Asterisks show absolute ages of craters in the Apollo landing sites Cross-shaded symbols indicate the crater lifetimes deduced from crystallization ages of mare lavas (Trask, 1971). Thick gray lines show trajectories of changing of crater diameters in the process of their maturation. (Modified from Basilevsky, 1976, 2015).

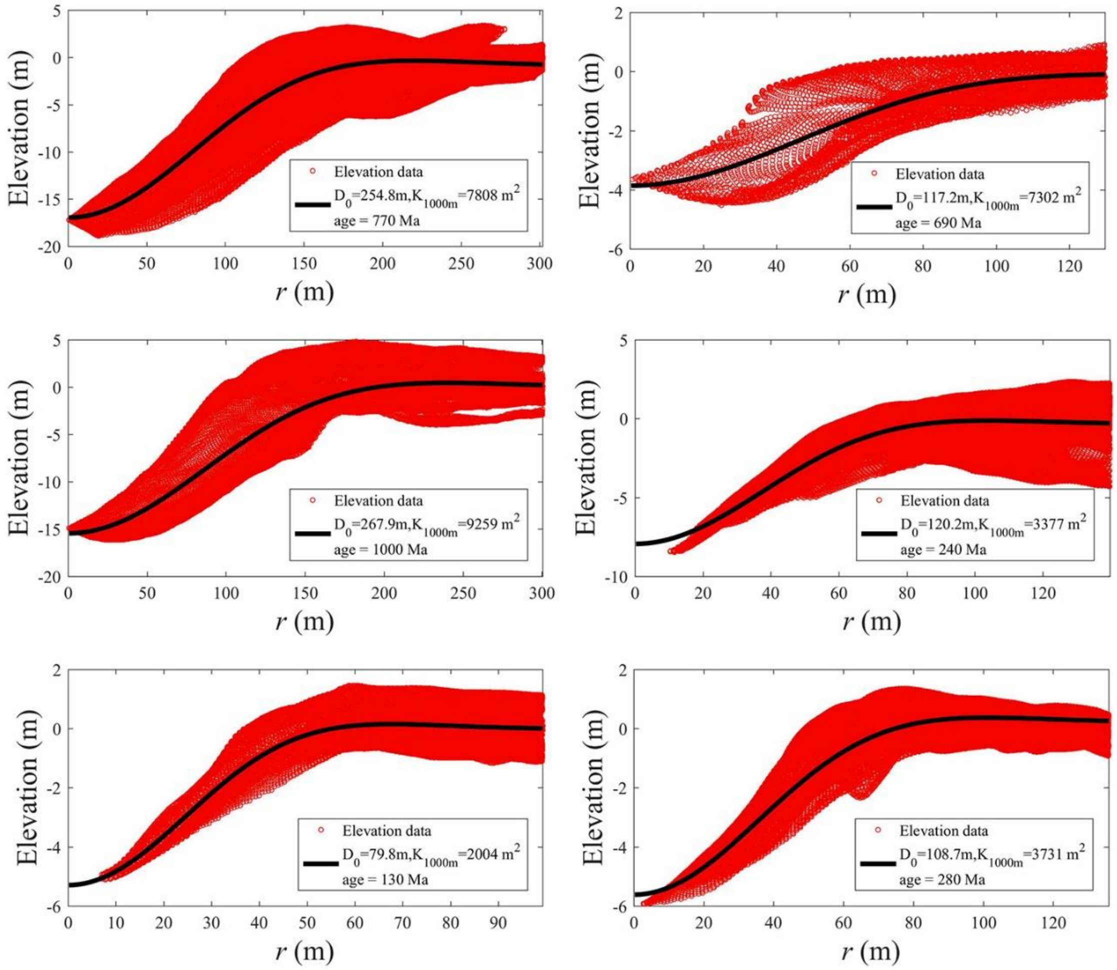

Figure 5. The crater profiles (the black curves) best-fit to the observed crater profiles (the red circles) extracted from NAC-based DTMs, corresponding to the individual cases illustrated in Figure 2. The ages of RMDS-superposed craters range from 130 to 1000 Ma. D_0 is the original diameter, and K_{1000m} is the diffusion age of a crater with a diameter of 1000 m derived by using Equation (2) in this study.

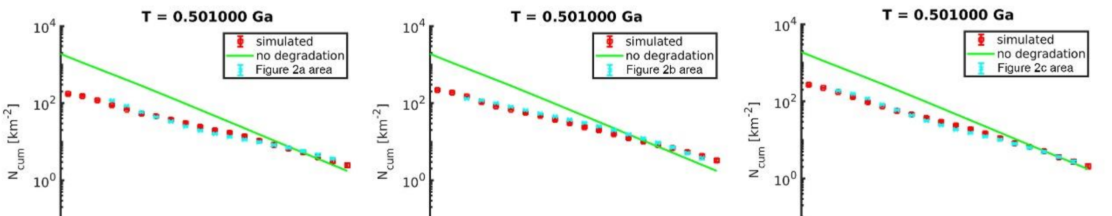

Figure 6. Modeled vs. simulated CSFDs in equilibrium after 0.5 Ga for square sub-regions of about 60 km^2 located inside the areas containing the RMDS-impact crater embayment respectively shown in Figures 2a-2c, obtained with the median values of κ_{10} and κ_{100} inferred by Bayesian optimization, respectively. The green lines correspond to the degradation-free CSFDs following from Neukum et al. (2001).

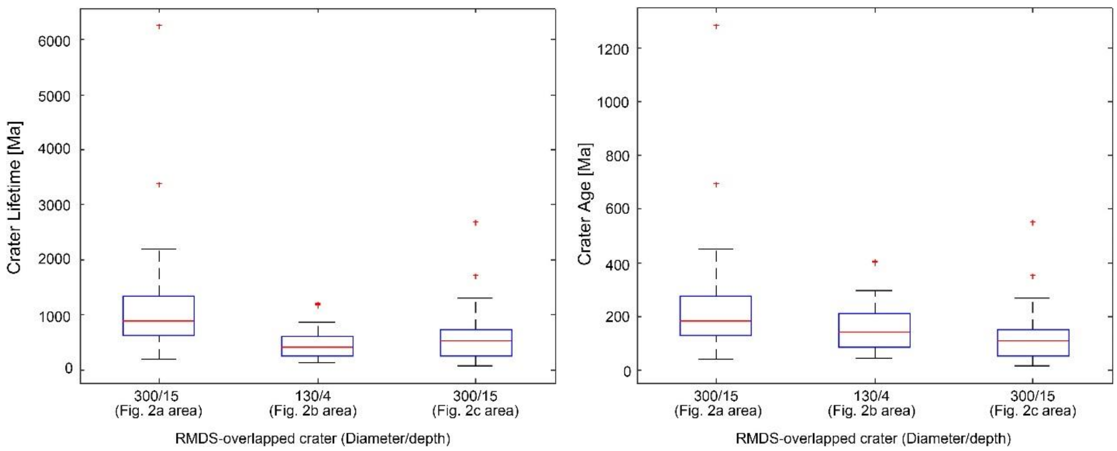

Figure 7. Boxplot representations of the crater lifetimes and ages for the RMDS-overlapped craters, as shown in Figures 2a-2c, respectively. Red lines denote median values, blue boxes the 25% and 75% quantiles, and whiskers the most extreme values of the distribution which are not outliers. Red crosses mark outliers, where the Bayesian optimization was unable to find a solution.

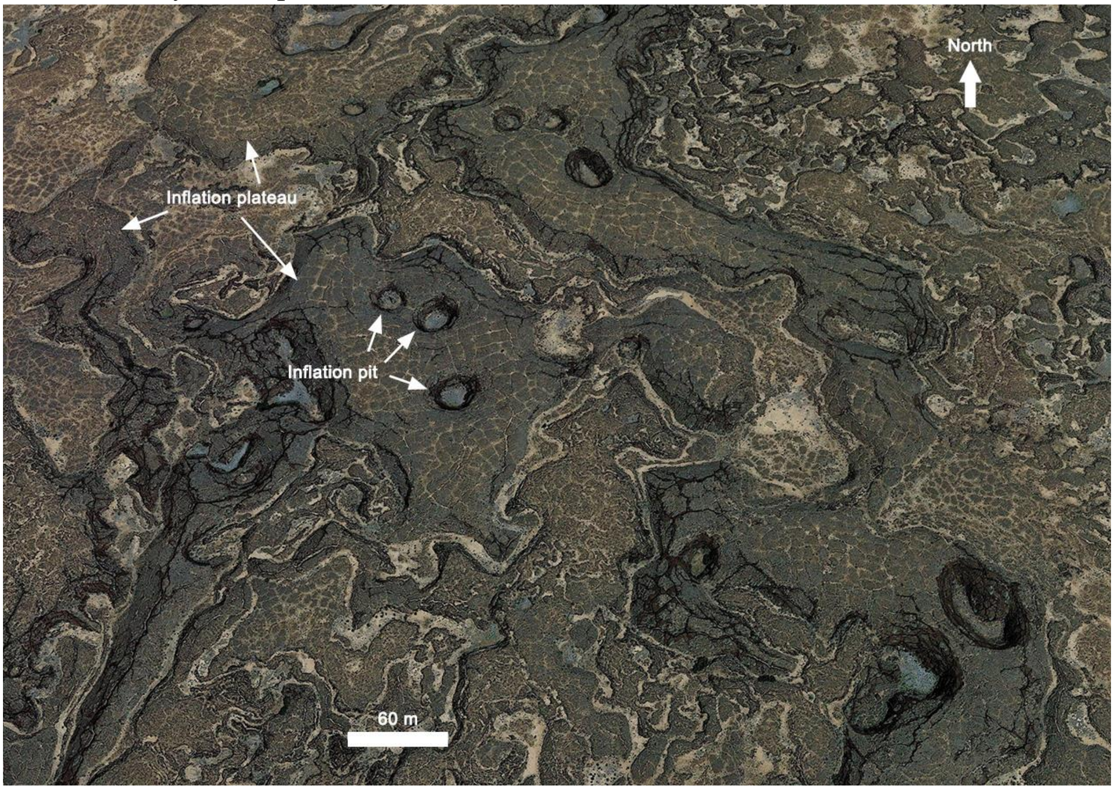

Figure 8. Terrestrial analogs of crater-like formations: Above aerial view of a group of circular depressions interpreted as lava-rise (or inflation) pits (De Hon & Earl, 2018), Aden Basalt. Satellite image credit: Google Earth.

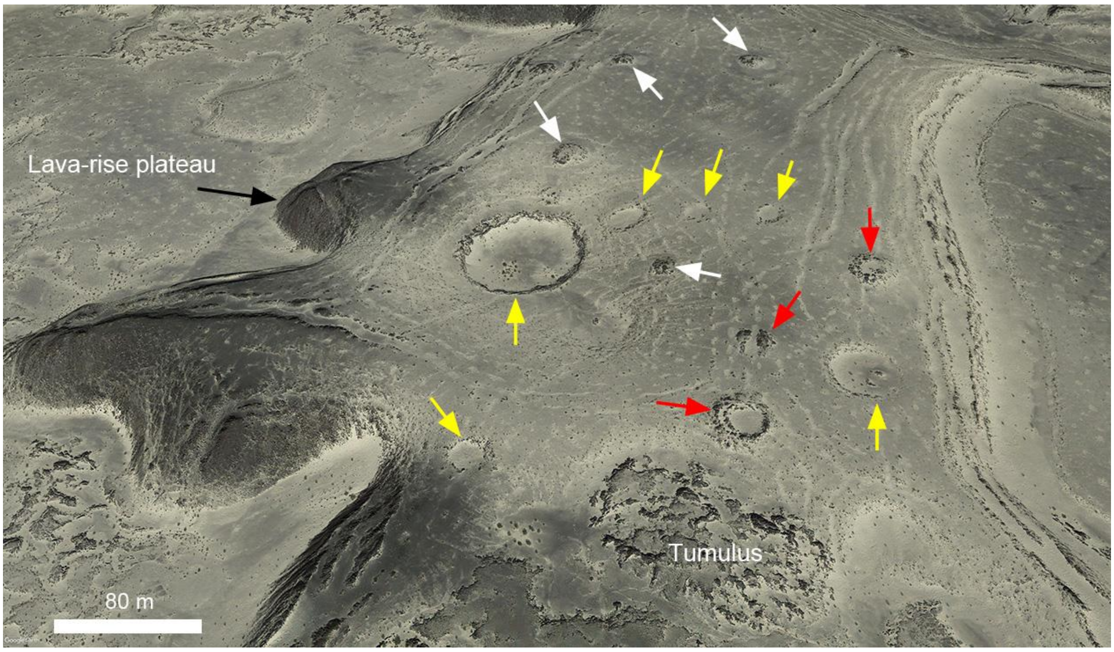

Figure 9. Oblique view of a series of positive and negative features on inflation (pressure, or lava-rise) plateau surface in the inflated Amboy lava flow field (Location: 34.5330°N, 115.8220°W), Mojave Desert, California. Yellow arrows indicate crater-like forms, while white arrows point to nearly circular tumulus-like structures. Red arrows illustrate three tumulus-like structures that have been degraded to varying degrees. The red arrow in the bottom presents a raised rim crater interpreted in this study as a collapsed tumulus. Image credit: Google Earth. North is up.

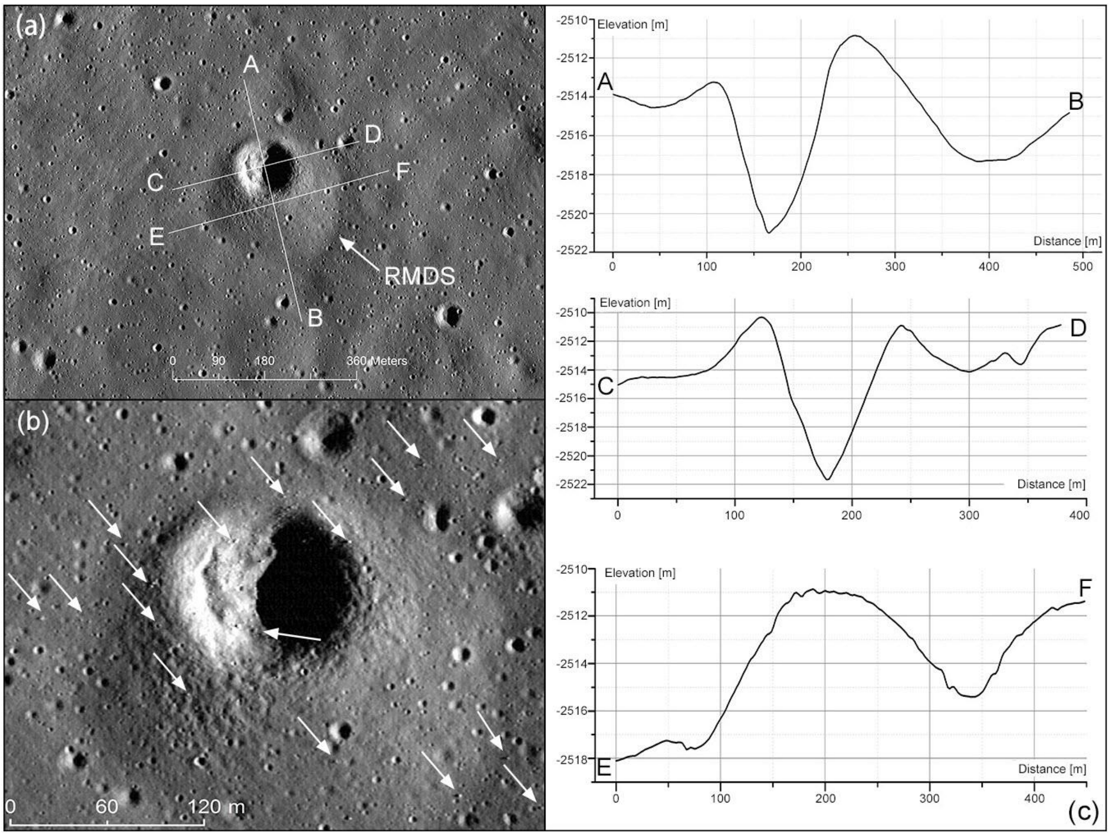

Figure 10. The 120-m crater is superposed on the northern part of a 270 m RMDS in Mare Fecunditatis (NAC frame: M131284180LE). (a) The RMDS-Crater relationship seen from LROC NAC with sun illumination direction from right to left. (b) The presence of meter-sized rock boulders (white arrows) on the crater rim and floor. (c) NAC-DEM-based topographic files extracted along the white lines AB, CD, and EF indicated in Figure (a). North is up in Figures (a) and (b).

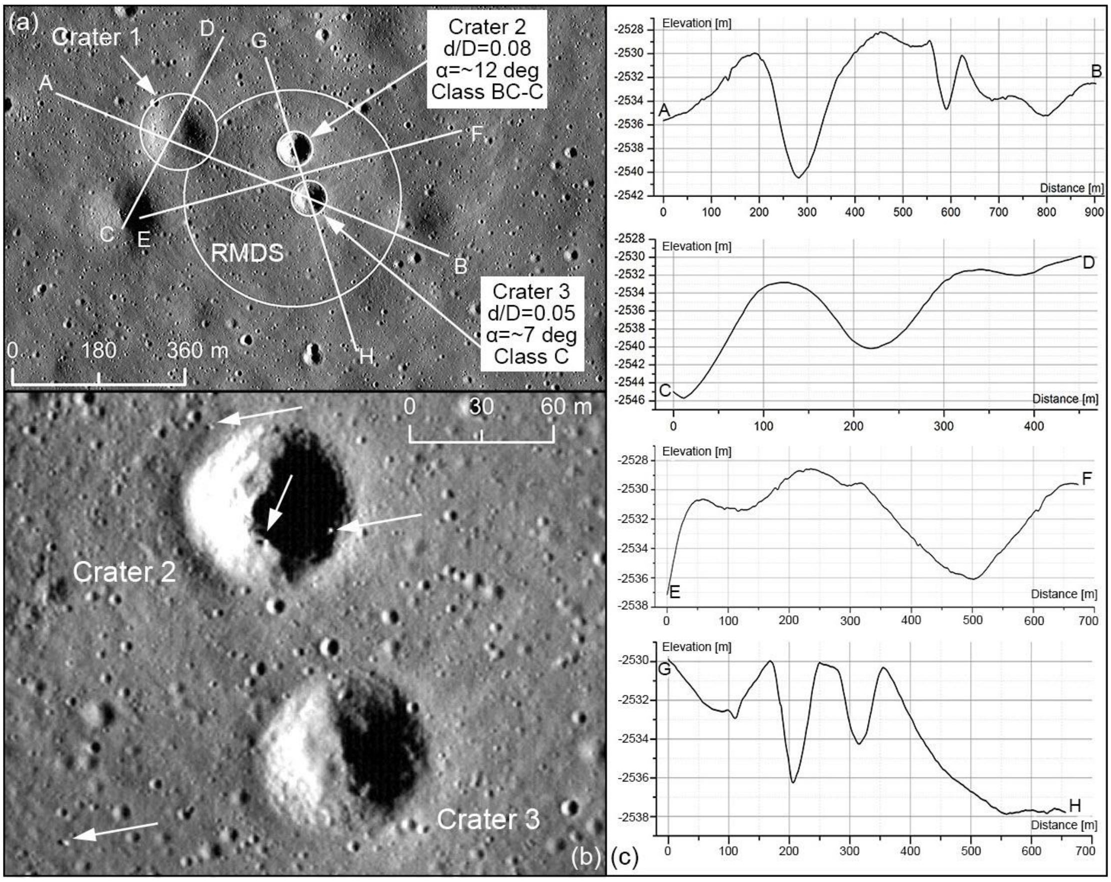

Figure 11. Three craters, 170, 80 and 80 m in diameter are superposed on a ~450-m RMDS in Mare Fecunditatis (NAC frame: M131284180RE). (a) The RMDS-Crater relationship seen from LROC NAC with sun illumination direction from right to left. (b) Meter-sized rock boulders (white arrows) are seen on the rim and floor of crater 2. (c) NAC-DEM-based topographic files extracted along the white lines AB, CD, EF, and GH indicated in Figure (a). North is up in Figures (a) and (b).

Table 1. Diffusion rates κ_{10} and κ_{100} for craters of 0.01 and 0.1 km diameter, respectively, for the three areas located close to the RMDS-overlapped craters in Figures 2a-2c, as derived with the locally calibrated diffusion-based method described in section 4.3. The values correspond to the median over 30 simulation runs and 25% and 75% quantiles, respectively.

area	$\boldsymbol{\kappa_{10}}$ $[\mathbf{m^2/Ma}]$	$\boldsymbol{\kappa_{100}}$ $[\mathbf{m^2/Ma}]$
Fig. 2a	$2.21^{+0.35}_{-0.29}$	$11.6^{+2.03}_{-2.99}$
Fig. 2b	$1.91^{+0.62}_{-0.39}$	$8.24^{+4.51}_{-2.31}$
Fig. 2c	$1.44^{+0.39}_{-0.41}$	$14.2^{+7.45}_{-2.21}$

Table 2. Statistical results for the diameter (D), depth (d), and inner slope (α) information of the small craters partially superposed by RMDSs, and their model ages measured from their morphologic analysis (Basilevsky, 1976; Figure 4) and the topographical diffusion model (Figure 5) used in this study.

ID	**Figure**	**Crater Center Location (Lon, Lat)**	**Crater Diameter (D, m)**	**Crater depth (d, m)**	**Maximum Inner slope** (α, °)	**Degradation age (Ma) by Basilevsky (1976)**	**Topographical diffusion model age (Ma) in this study**
1	Fig. 2a	27.451, 5.936	~300	~15	~9	750-1500	770
2	Fig. 2b	-37.294, -22.970	~130	~4	~6-8	160-320	690
3	Fig. 2c	52.393, -1.456	~300	~15	~9	750-1500	1000
4	Fig. 2d	34.187, 6.029	~140	~7-9	~8-9	200-300	240
5	Fig. 2e	-27.224, 30.703	~100	~5-6	~8-10	200-300	130
6	Fig. 2f	-27.083, 29.884	~135	~5-7	~7-8	200-300	280

Journal of Geophysical Research: Planets

Supporting Information for

The Lunar Mare Ring-Moat Dome Structure (RMDS) Age Conundrum: Contemporaneous with Imbrian-Aged Host Lava Flows or Emplaced in the Copernican?

Feng Zhang[1,2], James W. Head[3], Christian Wöhler[4], Alexander T. Basilevsky[5], Lionel Wilson[6], Minggang Xie[7], Roberto Bugiolacchi[2], Thorsten Wilhelm[4], Stephanie Althoff[4], and Yong L. Zou[1]

[1]State Key Laboratory of Space Weather, National Space Science Center, Chinese Academy of Sciences, Beijing, China; [2]State Key Laboratory of Lunar and Planetary Sciences, Macau University of Science and Technology, Macau, China; [3]Department of Earth, Environmental and Planetary Sciences, Brown University, Providence, RI, USA; [4]Image Analysis Group, TU Dortmund University, Dortmund, Germany; [5]Vernadsky Institute of Geochemistry and Analytical Chemistry, Russian Academy of Sciences, Moscow, Russia; [6]Lancaster Environment Centre, Lancaster University, Lancaster, UK; [7]College of Science, Guilin University of Technology, Guilin, China

Contents of this file

Introduction

The images were processed and investigated using the software ArcGIS 10.6. Topography data and elevation measurements were derived from DTMs on LROC NAC images/sets.

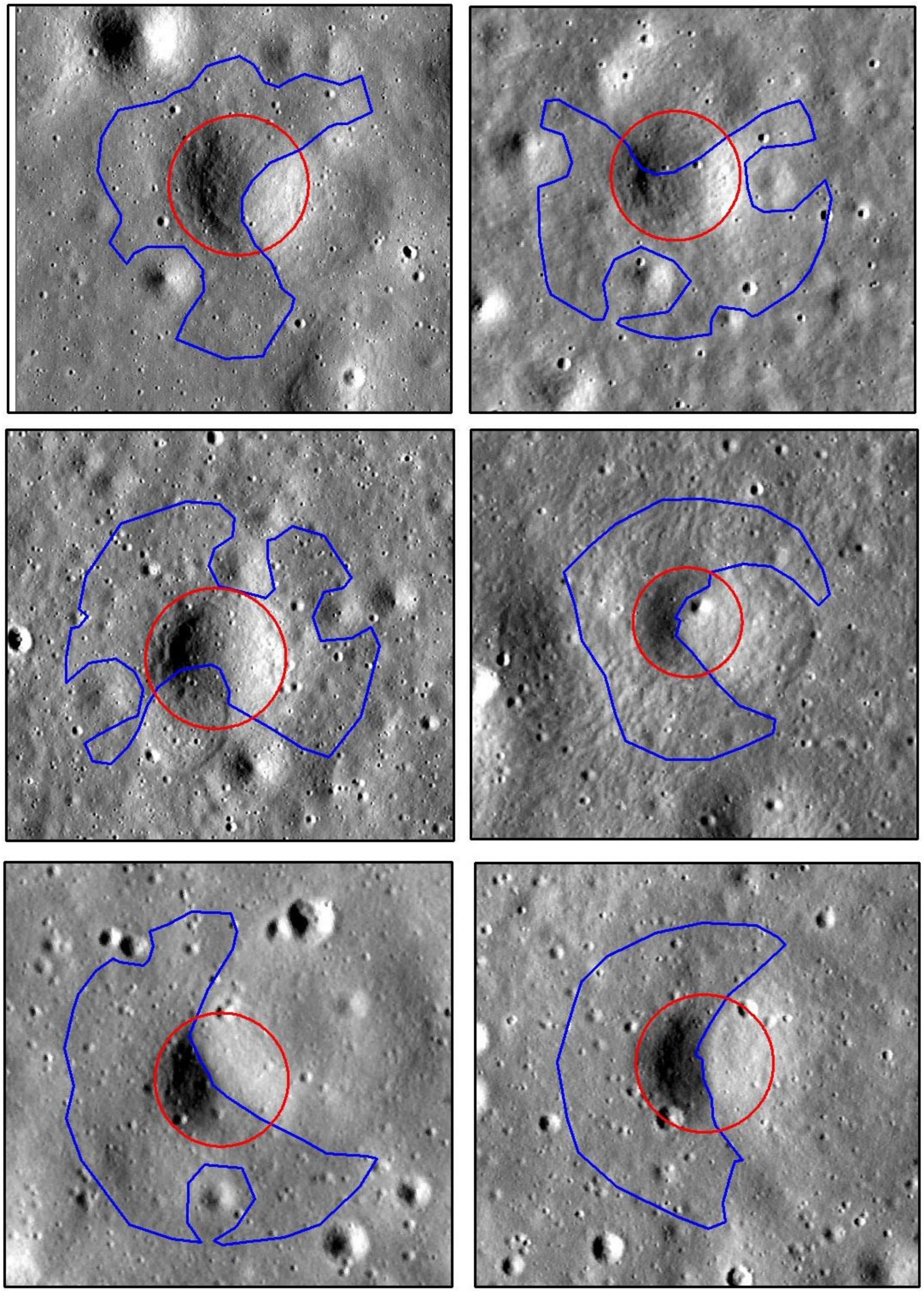

Figure S1: NAC images showing RMDS-superposed craters (Red circles). The pre-impact surface is constructed by fitting a plane to the elevation data beyond 1.5 radii from crater center. The regions used for the extraction of crater topography are shown in blue polygons.

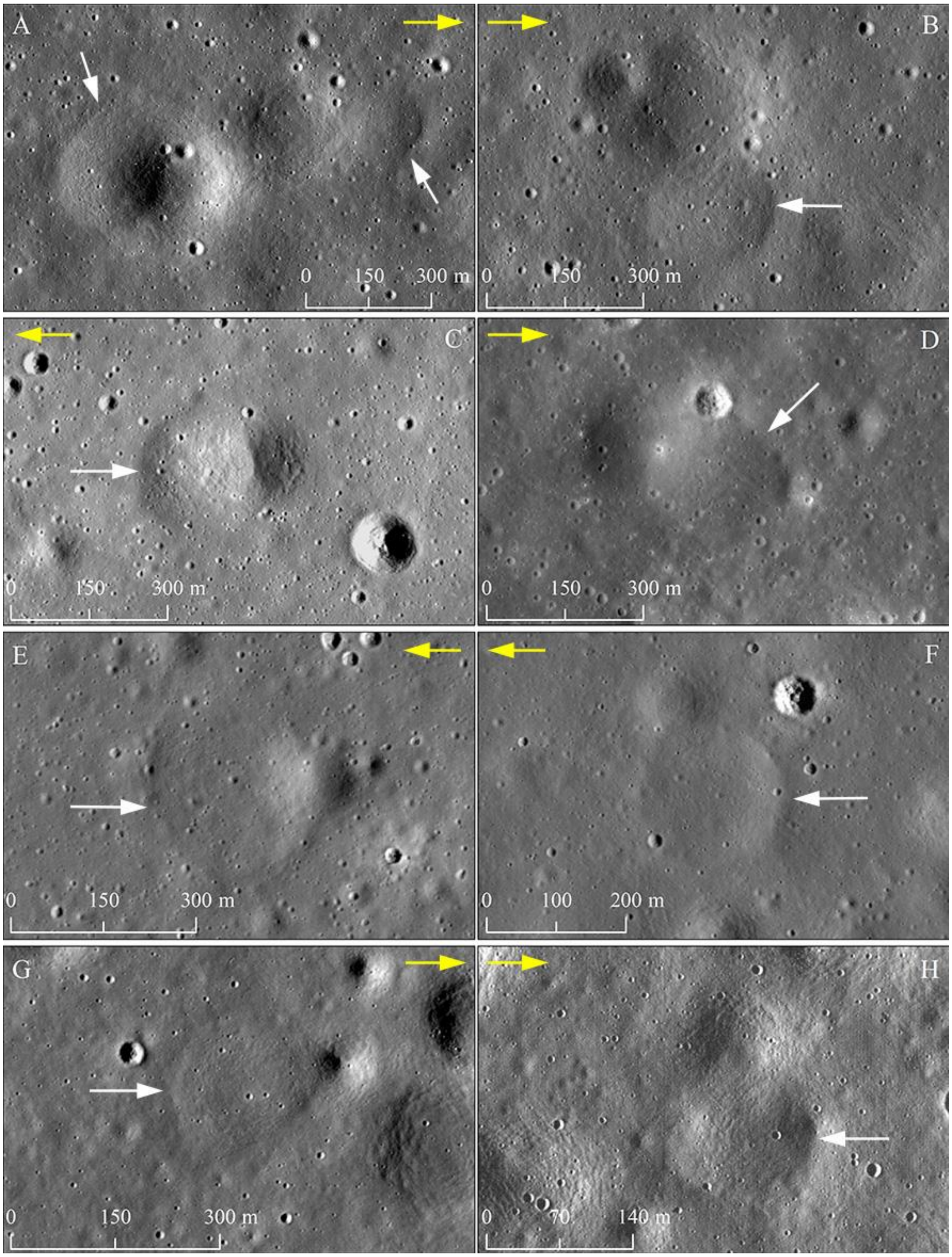

Figure S2: LROC NAC images for some candidate RMDS-crater overlap relationships.
(A) Location: 6.506°N, 34.177°E; Tranquillitatis, NAC frame M180944663RE.
(B) Location: 8.276°S, 49.525°E; Fecunditatis, NAC frame M1188038662RE.
(C) Location: 0.937°S, 52.398°E; Fecunditatis, NAC frame M1245671393LE.
(D) Location: 0.234°S, 55.944°E; Fecunditatis, NAC frame M183160424LE.
(E) Location: 29.288°N, 28.047°W; Imbrium, NAC frame M1139086679LE.
(F) Location: 6.38°S, 40.459°W; Procellarum, NAC frame M131914933RE.
(G) Location: 22.634°S, 38.306°W; Humorum, NAC frame M1142688086RE.
(H) Location: 22.832°S, 38.091°W; Humorum, NAC frame M133079100RE.

Yellow arrows point to sun illumination directions, while white arrows point to RMDSs. North is up in all figures.

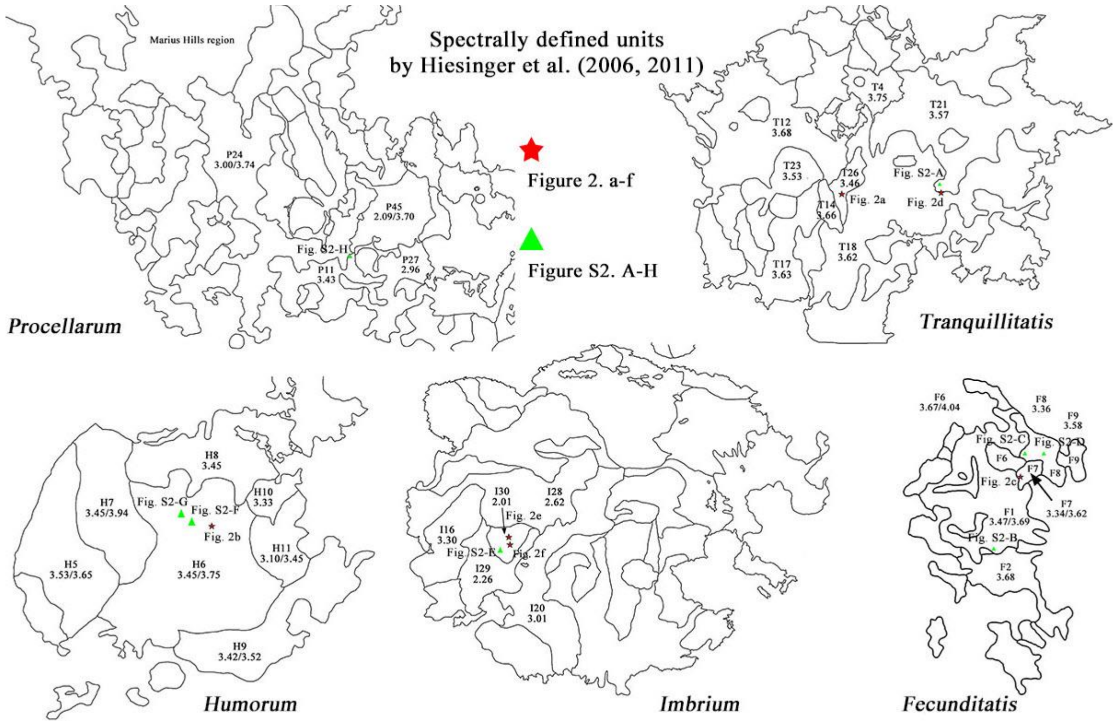

Figure S3: Distribution of RMDS-superposed craters on the nearside maria. Red stars represent the cases in Figure 1, while green triangles illustrate the cases in Figure S1. The black lines indicate spectrally defined units by Hiesinger et al. (2006, 2011). For some mare units hosting RMDS-superposed craters, their names and model ages (Hiesinger et al., 2006, 2011) by crater size-frequency measurement are labeled. Generally, these mare units containing the RMDSs shown in Figures 2 and S2 are of > 3.0 Ga in age, with an exception of the mare unit in Mare Imbrium which was dated to be ~2.0 Ga ago.

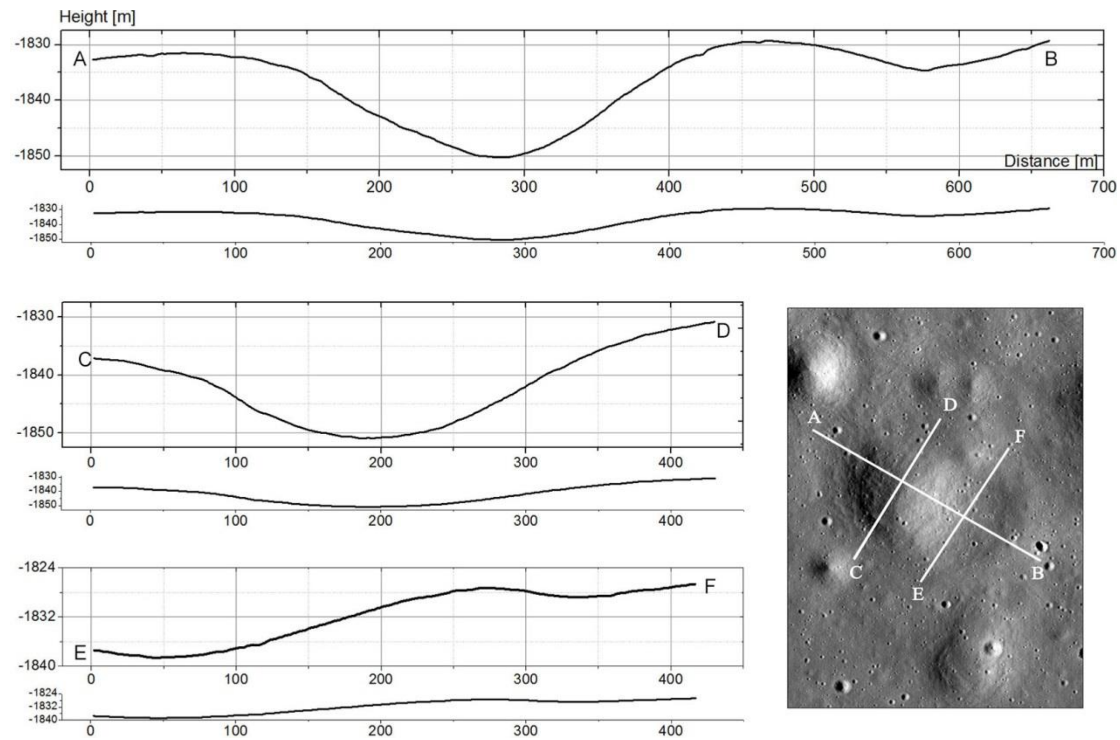

Figure S4: NAC-DEM based topographic profiles (a respective more and less vertically exaggerated profiles) of the RMDS-superposed crater shown in Figure 2a.

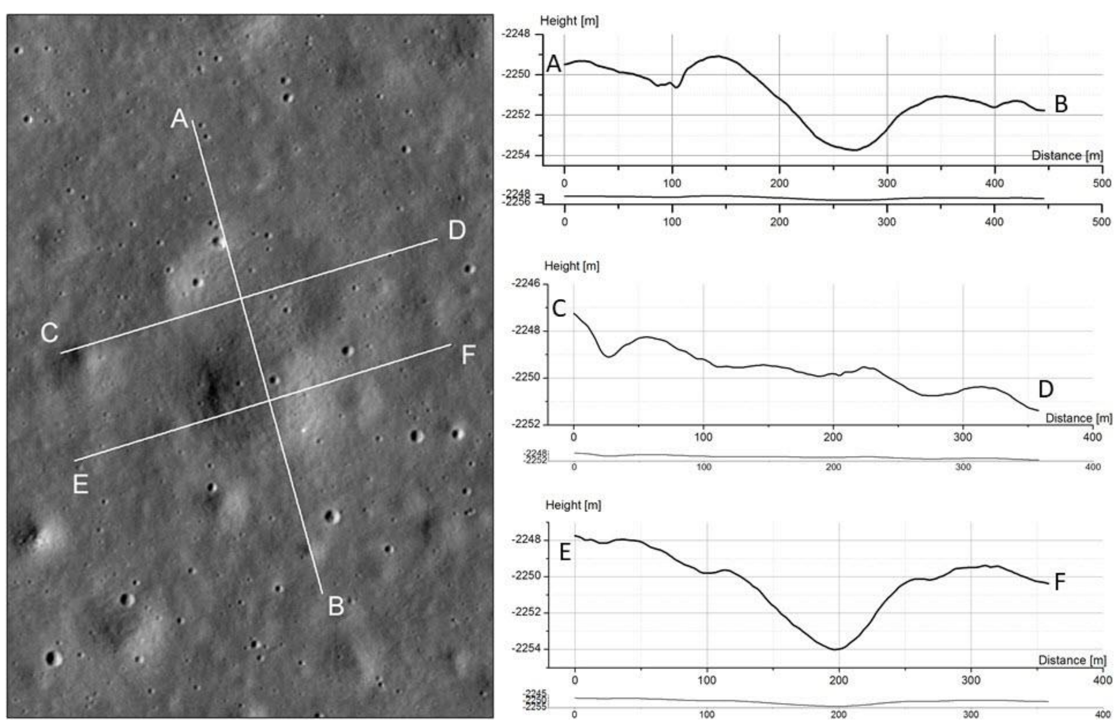

Figure S5: NAC-DEM based topographic profiles (a respective more and less vertically exaggerated profiles) of the RMDS-superposed crater shown in Figure 2b.

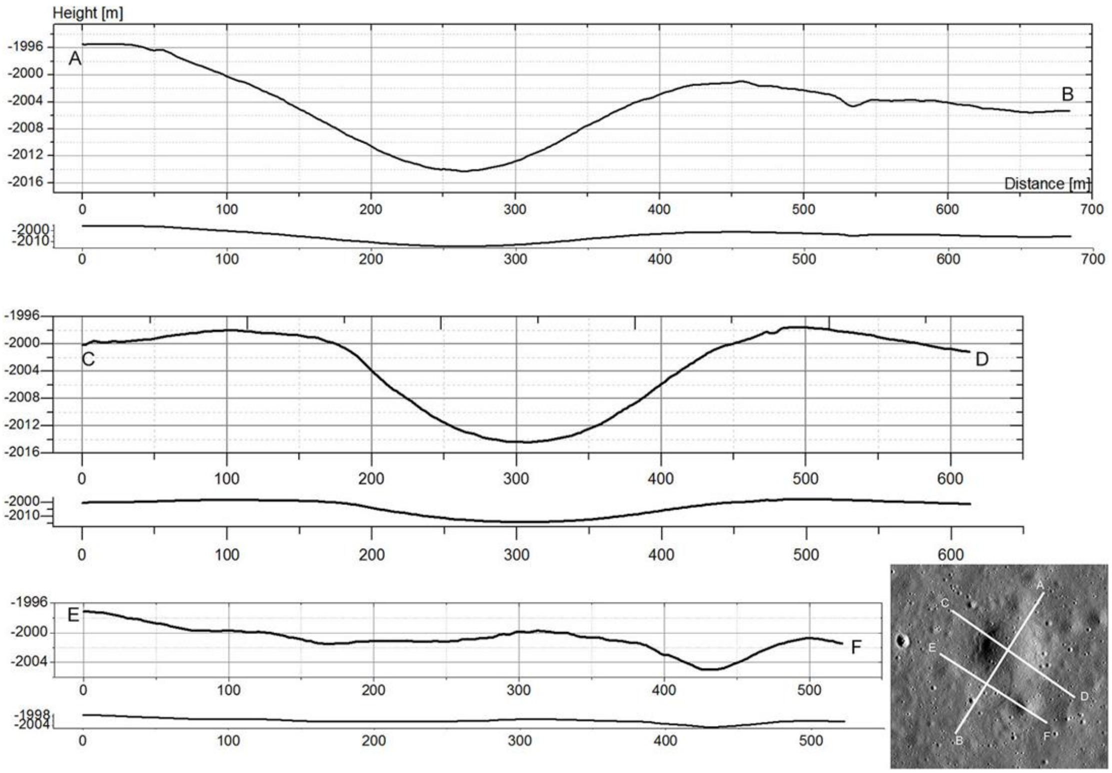

Figure S6: NAC-DEM based topographic profiles (a respective more and less vertically exaggerated profiles) of the RMDS-superposed crater shown in Figure 2c.

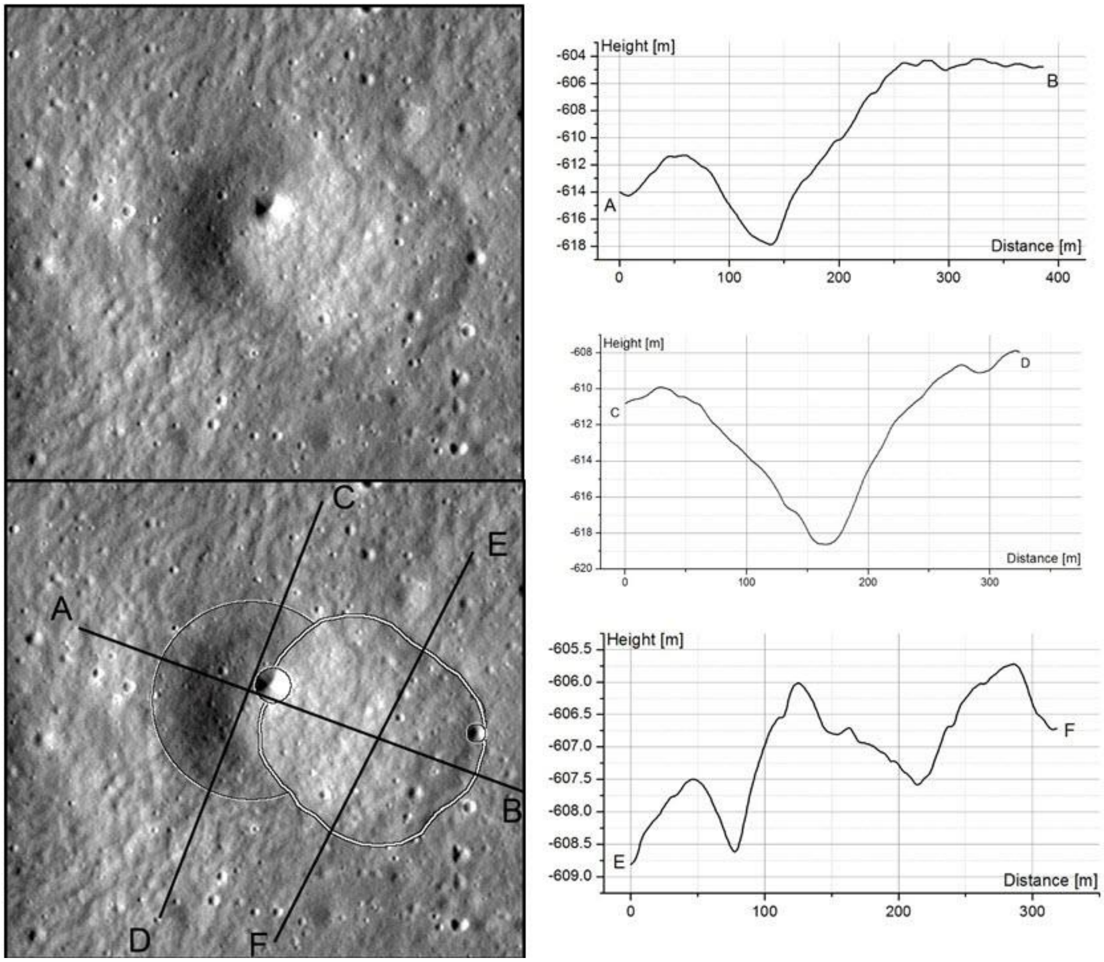

Figure S7: NAC-DEM based topographic profiles (a respective more and less vertically exaggerated profiles) of the RMDS-superposed crater shown in Figure 2d.

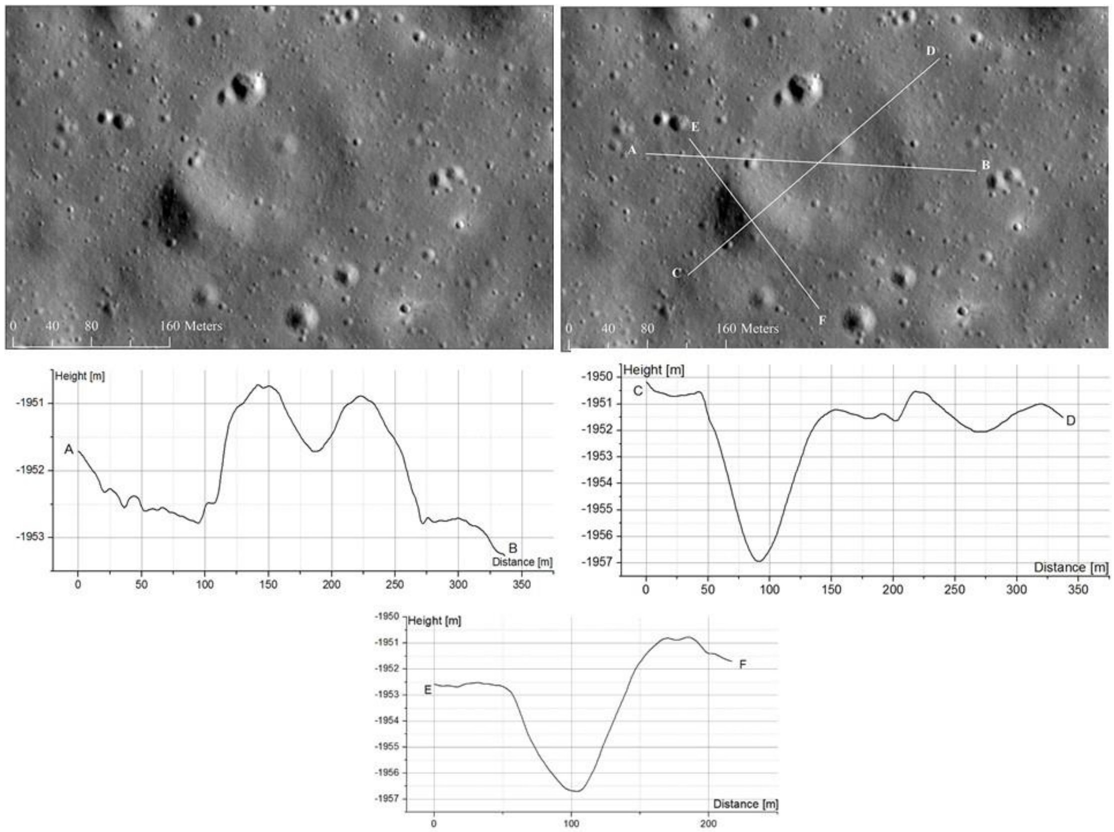

Figure S8: NAC-DEM based topographic profiles (a respective more and less vertically exaggerated profiles) of the RMDS-superposed crater shown in Figure 2e.

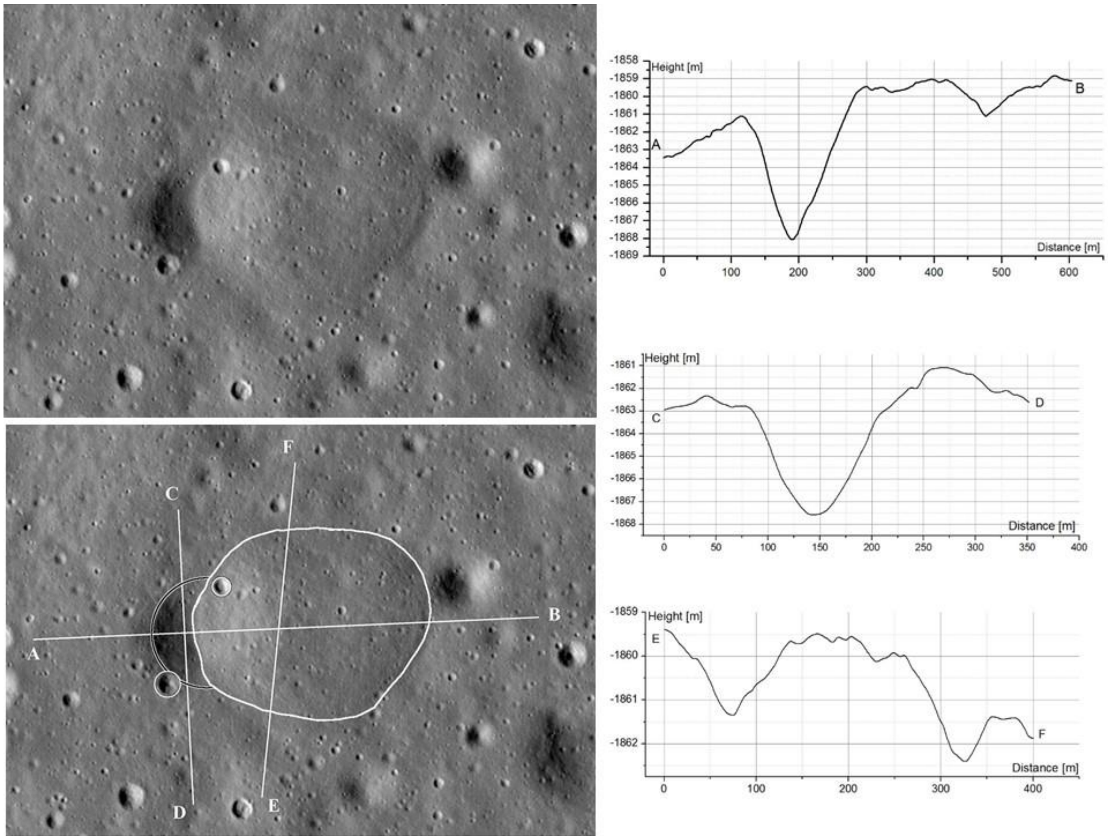

Figure S9: NAC-DEM based topographic profiles (a respective more and less vertically exaggerated profiles) of the RMDS-superposed crater shown in Figure 2f.

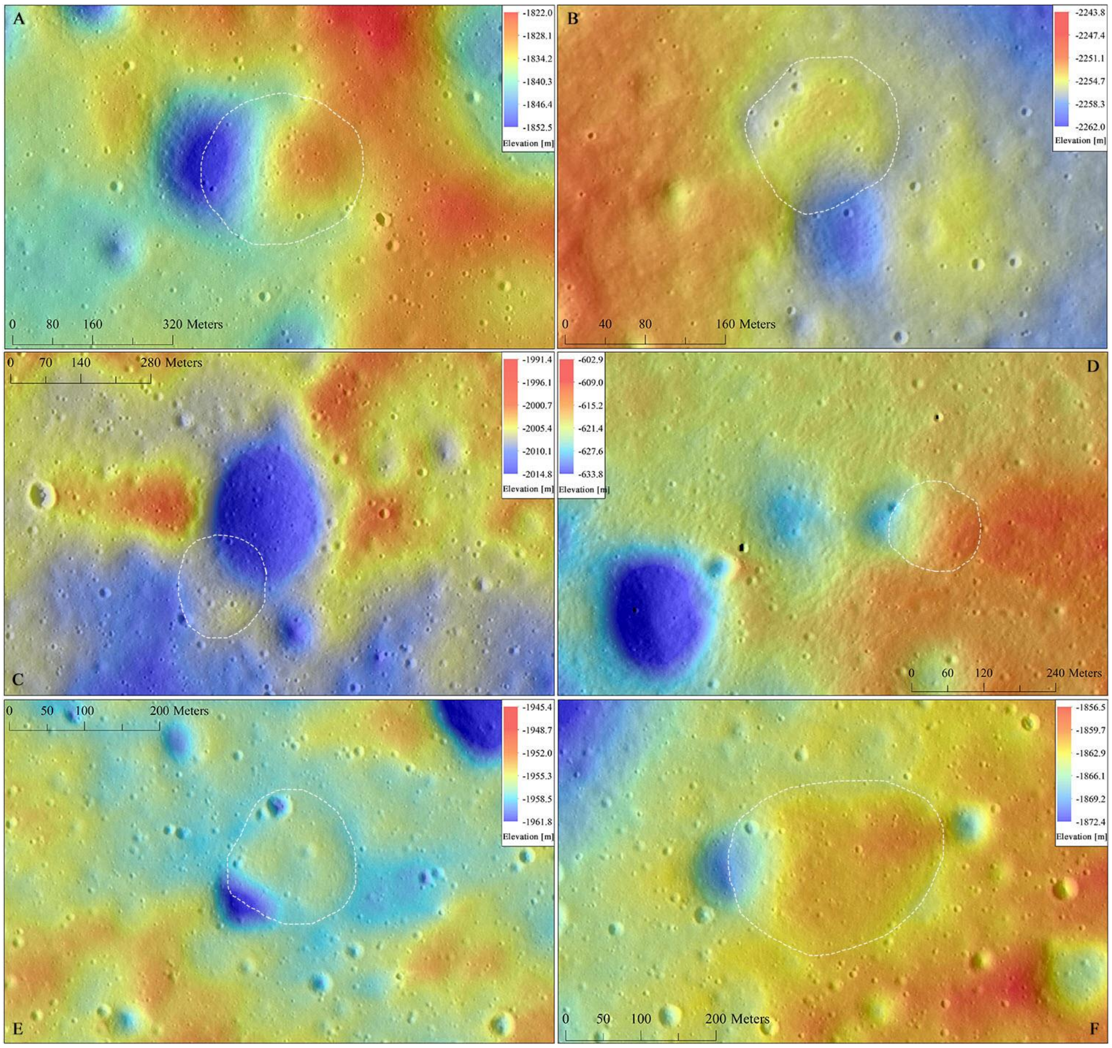

Figure S10: LROC NAC-derived 2 m/pixel DTM for each of RMDS-superposed crater used in this study. An approximate outline of each RMDS is illustrated by dashed white line in each subfigure. NAC image pairs used to construct DTMs are included: (A) M1172873803LE and RE; (B) M1142680981LE and RE; (C) M1126787189LE and RE; (D) M180944663LE and RE; (E) and (F) M181352550LE and RE.